# A new member of the dynamin superfamily modulates mitochondrial membrane branching in Trypanosoma brucei.

Chloé Alexandra Morel, Corinne Asencio, David Moreira, Corinne Blancard, Bénédicte Salin, Étienne Gontier, S. Duvezin-Caubet, Manuel Rojo, Frederic Bringaud, Emmanuel Tetaud

Article

Current Biology

# A new member of the dynamin superfamily modulates mitochondrial membrane branching in *Trypanosoma brucei*

## Graphical abstract

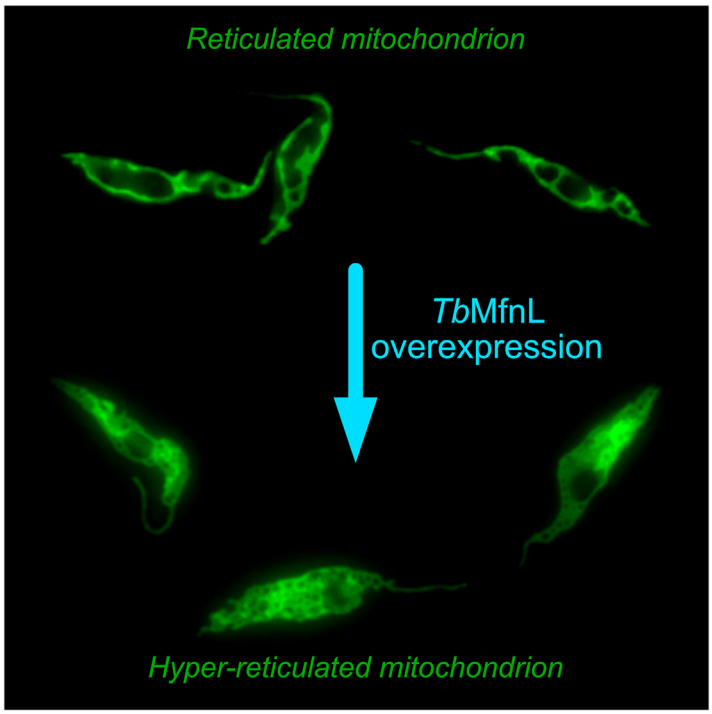


## Highlights

- *Tb*MfnL is a dynamin-related protein anchored to the inner mitochondrial membrane
- *Tb*MfnL modulates the branching of mitochondrial networks in a GTPase-dependent manner
- *Tb*MfnL is phylogenetically distant from dynamin-related proteins of opisthokonts
- *Tb*MfnL is part of a new membrane remodeling machinery of eukaryotes and prokaryotes

## Authors

Chloé Alexandra Morel, Corinne Asencio, David Moreira, ..., Manuel Rojo, Frédéric Bringaud, Emmanuel Tetaud

## Correspondence

emmanuel.tetaud@u-bordeaux.fr

## In brief

The mitochondria of trypanosomes form a single interconnected network. Morel et al. identify *Tb*MfnL, a new member of the dynamin superfamily protein in *T. brucei* that modulates inter-mitochondrial branching. *Tb*MfnL is a transmembrane protein exposed to the matrix that is phylogenetically distant from yeast and mammalian dynamin-related proteins.

Morel et al., 2025, Current Biology *35*, 1–16
March 24, 2025 
https://doi.org/10.1016/j.cub.2025.02.033

CellPress

Current Biology

CellPress
OPEN ACCESS

Article

# A new member of the dynamin superfamily modulates mitochondrial membrane branching in *Trypanosoma brucei*

Chloé Alexandra Morel,[1] Corinne Asencio,[1] David Moreira,[2] Corinne Blancard,[3] Bénédicte Salin,[3] Etienne Gontier,[4] Stéphane Duvezin-Caubet,[3] Manuel Rojo,[3] Frédéric Bringaud,[1] and Emmanuel Tetaud[1,5,*]

[1]Univ. Bordeaux, CNRS, MFP, UMR 5234, F-33000 Bordeaux, France
[2]Ecologie Systématique Evolution, CNRS, Université Paris-Saclay, AgroParisTech, 91190 Gif-sur-Yvette, France
[3]Univ. Bordeaux, CNRS, IBGC, UMR 5095, F-33000 Bordeaux, France
[4]Univ. Bordeaux, CNRS, INSERM, BIC, US4, UAR 3420, F-33000 Bordeaux, France
[5]Lead contact
*Correspondence: emmanuel.tetaud@u-bordeaux.fr
https://doi.org/10.1016/j.cub.2025.02.033

## SUMMARY

Unlike most other eukaryotes, where mitochondria continuously fuse and divide, the mitochondrion of trypanosome cells forms a single and continuously interconnected network that divides only during cytokinesis. However, the machinery governing mitochondrial remodeling and interconnection of trypanosome mitochondrion remain largely unknown. We functionally characterize a new member of the dynamin superfamily protein (DSP) from *T. brucei* (*Tb*MfnL), which shares similarity with a family of homologs present in various eukaryotic and prokaryotic phyla but not in opisthokonts like mammals and budding yeast. The sequence and domain organization of *Tb*MfnL is distinct, and it is phylogenetically very distant from the yeast and mammalian dynamin-related proteins involved in mitochondrial fusion/fission dynamics, such as optic atrophy 1 (Opa1) and mitofusin (Mfn). *Tb*MfnL localizes to the inner mitochondrial membrane facing the matrix and, upon overexpression, induces a strong increase in the interconnection and branching of mitochondrial filaments in a GTPase-dependent manner. *Tb*MfnL is a component of a novel membrane remodeling machinery with an unprecedented matrix-side localization that is able to modulate the degree of inter-mitochondrial connections.

## INTRODUCTION

*Trypanosoma brucei* is a parasite responsible for African sleeping sickness as well as the related cattle disease Nagana, affecting sub-Saharan Africa. *T. brucei* is transmitted to mammals by an insect vector: the tsetse fly (*Glossina* spp.). During the trypanosome life cycle, the parasite exists in at least two replicative forms: the procyclic form (PCF), transmitted by the tsetse fly, and the bloodstream form (BSF), responsible for diseases in vertebrates. Unlike most other eukaryotes that contain numerous mitochondria, trypanosomes have a single mitochondrion, which is often elongated and reticulated. In contrast to yeast and mammals, with tens to hundreds of mitochondrial DNA (mtDNA) nucleoids distributing throughout the mitochondrial compartment, the mitochondrial genome of trypanosomes is restricted to a specific structure at the base of the flagellum known as kinetoplast DNA (kDNA).[1] During the trypanosome life cycle and its adaptation to different hosts and environments, the shape of its mitochondrial compartment undergoes spectacular changes that reflect its functional plasticity.[2] Indeed, the mitochondrion of this parasite exists in at least two major forms: (1) the fully active and developed one characteristic for the PCF that harbors the oxidative phosphorylation (OXPHOS) complexes for energy production[3,4] and (2) the functionally less active and morphologically reduced form found in the bloodstream, with energy produced mainly through glycolysis since OXPHOS is repressed.[5] These modifications correlate with the adaptation of the parasite to the proline-rich hemolymph and tissue fluids of the blood-feeding tsetse fly and the glucose-rich blood of a mammalian host.[6] Since studies in mammals and in yeast have unraveled tight links between mitochondrial bioenergetics, morphology, and dynamics,[7–9] it is tempting to assume that such close relationships not only regulate mitochondrial function and energy metabolism but also the life cycle and pathogenic potential of trypanosomes. However, in contrast to fungi and metazoa, where mitochondrial morphology and fusion/fission dynamics have been thoroughly characterized,[10,11] little is known about the morphology and dynamics of mitochondria in trypanosomes.

In most eukaryotes, mitochondria are very dynamic, alternating between two major events, fusion and fission. Mitochondrial dynamics allows the maintenance of mitochondrial morphology, distribution, and size.[8] The main proteins involved in these events are large GTPases belonging to the dynamin superfamily protein (DSP), such as Dnm1/Drp1 in yeast and mammalian cells, which are soluble proteins transiently recruited

Please cite this article in press as: Morel et al., A new member of the dynamin superfamily modulates mitochondrial membrane branching in *Trypanosoma brucei*, Current Biology (2025), https://doi.org/10.1016/j.cub.2025.02.033



to mitochondrial and peroxisomal membranes to mediate organelle division.[12,13] Mammalian mitochondrial fusion requires fusion of the outer mitochondrial membrane followed by fusion of the inner mitochondrial membrane, which is carried out by mitofusins 1 and 2 (Mfn1 and Mfn2) and optic atrophy 1 (Opa1), respectively.[14,15] While Mfns are anchored to the outer mitochondrial membrane and face the cytosol, Opa1 localizes to the mitochondrial intermembrane space. Alteration of fusion/fission dynamics and of the equilibrium between them provokes mitochondrial fragmentation or hyperfusion[12,16] and is linked to diseases, notably neuropathies.[17]

The investigation of mitochondrial fission and fusion in trypanosomes has been relatively limited until now. Available evidence indicates that mitochondrial fission is restricted to cell division[18,19] and may not occur continuously[18,20] but can be induced artificially.[19,21] Evidence for mitochondrial fusion in trypanosomes came 25 years ago from *in vivo* genetic exchange of mtDNA.[22] Finally, a recent study of mitochondrial dynamics in another trypanosomatid, *Crithidia fasciculata*, unveiled the occurrence of mitochondrial fission, fusion, and sliding throughout the cell cycle, pointing to the existence of mitochondrial fusion and fission machineries in trypanosomatids.[23]

Two decades of research have revealed that, despite significant differences, numerous mitochondrial fission and fusion factors appear conserved in fungi and mammals.[24] In plants, mitochondria also fuse and divide. While plant DSPs involved in fission are known, factors directly involved in fusion have not been identified, suggesting the existence of a fusion machinery differing from that of yeast and mammals.[25–27] So far, only two dynamin-like proteins (*Tb*Dlp) have been described in *T. brucei* (VEuPathDB: Tb927.3.4720 and Tb927.3.4760): their ablation impairs mitochondrial division and endocytosis and leads to cytokinesis arrest.[19,28,29] *Tb*Dlp thus appears to be the functional homolog of Drp1/Dnm1 in mammals and yeast, but its fission activity on mitochondria seems restricted to the cytokinesis.[19] Another presumed DSP (*Tb*MfnL, VEuPathDB: Tb927.7.2410) has also been reported to be involved in mitochondrial fission.[30] To date, however, no protein involved in mitochondrial fusion has been identified in trypanosomes.

In this study, we revisited the function of the trypanosome DSP *Tb*MfnL.[30] Phylogenetic analysis reveals that this protein defines a new family of DSP found in both eukaryotes and prokaryotes but absent from organisms containing Mfn or Opa1 homologs (fungi and mammals) and from plants. We find that excess *Tb*MfnL leads to increased mitochondrial branching and interconnection, and we show that it is anchored to the mitochondrial inner membrane, facing the matrix. Taken together, these findings suggest that *Tb*MfnL is not involved in fission but mediates or modulates mitochondrial interconnection and branching.

## RESULTS

### Sequence analysis of *Tb*MfnL identifies it as a member of a novel dynamin family

To identify potential fusion players, we started our search by careful re-examination of trypanosome genomic and proteomic databases for proteins showing sequence homology to known fusion factors (Opa1/Mfn1-2/Fzo1). We were only able to identify the previously reported dynamin-related protein, named *Tb*MfnL or *Tb*MfnL (VEuPathDB: Tb927.7.2410),[30] that displays a domain organization that has more similarities with mammalian and yeast fusion factors of the outer membrane (Mfn2/Fzo1) than of the inner membrane (Opa1) (Figure 1A; Table S1). Analysis of the *Tb*MfnL sequence revealed several motifs and domains, including an N-terminal region containing a predicted mitochondrial targeting signal (MTS) with potential cleavage sites (Figure S1), followed by a GTPase domain with conserved G1 to G4 motifs and two consecutive C-terminal transmembrane domains (TMs) (Figures 1A, S1, and S2). The presence of an N-terminal MTS makes it unlikely for *Tb*MfnL to localize to the outer membrane, as Mfn/Fzo, and the absence of an N-proximal TM, which prevents Opa1 import into the matrix, suggests that *Tb*MfnL is imported into the matrix and does not represent a functional homolog of the fusion factors Opa1 or Mfn. Although this protein is not the functional homolog of Mfn/Opa1, we have still retained its name (TbMfnL) to avoid any confusion in the literature.

We next investigated whether this DSP could be conserved in other organisms. Using Blastp with *Tb*MfnL as a query to search various protein databases, we identified well-conserved sequences in relatives of *Trypanosoma* belonging to the class Kinetoplastea, including free-living bodonid species (Figure S1; see Table S1 for examples). Surprisingly, we also discovered homologous proteins with high similarity across the entire sequence in other very diverse Euglenozoa species, including the classes Euglenida and Diplonemea, and also in various much more distantly related eukaryotic lineages, particularly within the SAR clade, including Stramenopiles and Alveolata (Figures 1B and S2; see Table S1 for example). However, no proteins with the same general architecture were identified in the Opisthokonta (the clade that includes fungi and animals) or in plants, the only sequences showing some similarity being restricted, as anticipated, to the well-conserved GTPase domain. Unexpectedly, we also identified several sequences similar to *Tb*MfnL in bacteria, mainly in the PVC group and in Proteobacteria (Figures 1B and S2; see Table S1 for example). Analysis of several of these proteins showed again a very conserved structural and domain organization along the whole sequence, with the exception of the absence of the potential MTS in prokaryotes (Figures 1B and S2).

We conducted a maximum likelihood phylogenetic analysis of the identified sequences, incorporating several DSPs from mammals and yeast, as well as the cyanobacterial homolog DBLP as outgroup sequences (Figures 1C and S3). Most eukaryotic sequences branched within a well-supported (99% ultrafast bootstrap support [UFBS]) group. Despite the fact that sequences within this clade tended to group according to their taxonomic origin, we observed several unexpected relationships (e.g., dinoflagellates branched within the Euglenozoa, and cryptophytes and haptophytes within the Stramenopiles). Moreover, colponemids (a group of deep-branching alveolates) formed a fully supported (100% UFBS) group with two stramenopile sequences. Bacterial sequences formed a paraphyletic group at the base of this main eukaryotic clade, with two amoebozoan species (*Acanthamoeba castellanii* and *Dracoamoeba jomungandri*) robustly branching (97% UFBS) within one of the bacterial subgroups. This unexpected relationship strongly suggested that these amoebae acquired this gene by horizontal gene transfer

Please cite this article in press as: Morel et al., A new member of the dynamin superfamily modulates mitochondrial membrane branching in *Trypanosoma brucei*, Current Biology (2025), https://doi.org/10.1016/j.cub.2025.02.033



CellPress
OPEN ACCESS

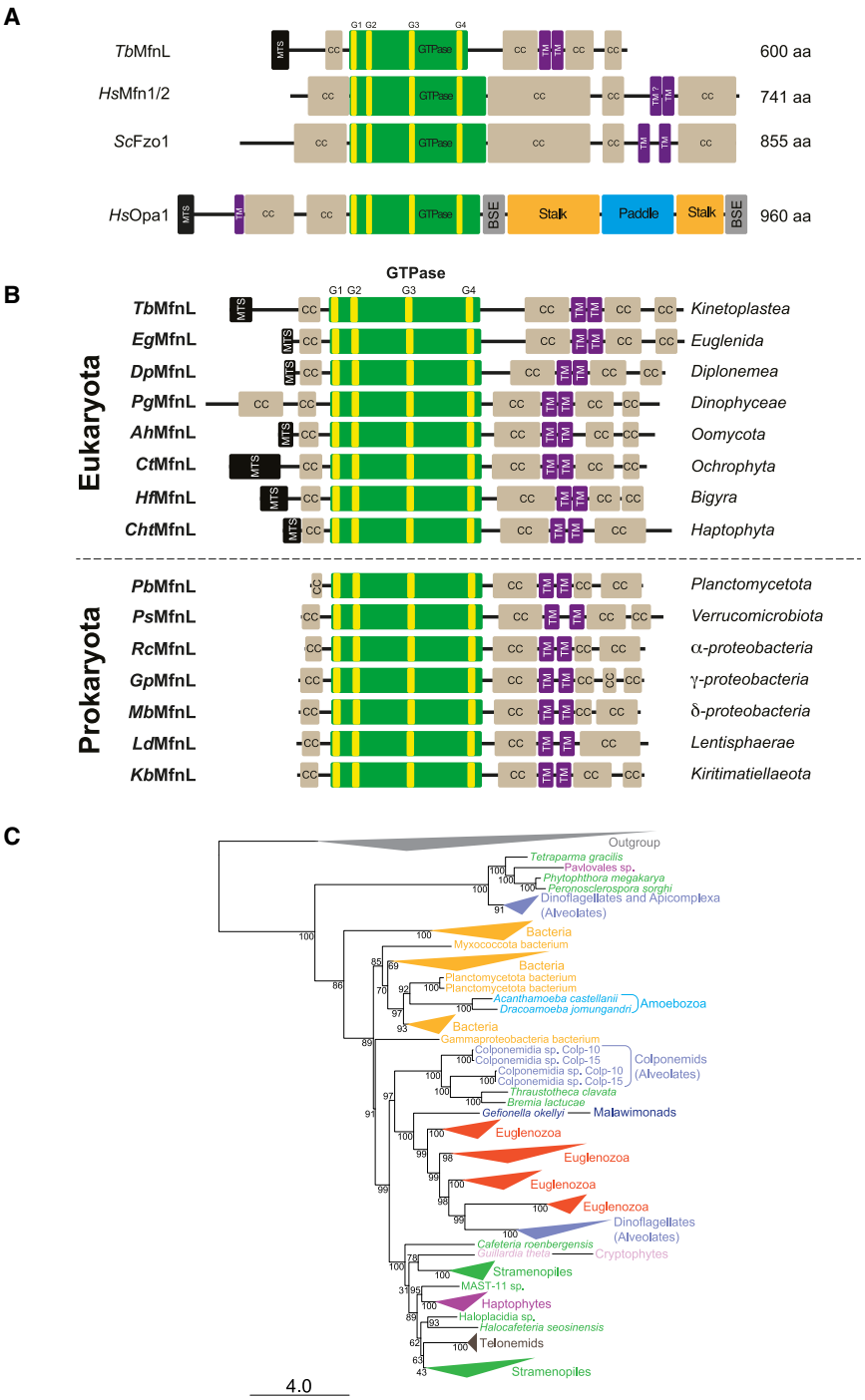


**Figure 1. Sequences homologous to *Tb*MfnL and domain organization of the proteins**

(A) Structure comparison between mitochondrial dynamin superfamily proteins (DSPs): *T. brucei* *Tb*MfnL, human mitofusin 1 or 2 (*Hs*Mfn1/2), yeast Fzo1 (*Sc*Fzo1), and human Opa1 (*Hs*Opa1). MTS, predicted mitochondrial targeting signal; CC, coiled-coil region; green box, GTPase domain with the four GTP-binding motifs in yellow; TM, transmembrane span; BSE, bundle signaling element; stalk domain; paddle domain. Two TMs were initially proposed for Mfn1/2, but recently, Mattie et al.[31] reported the presence of only a single TM, with the C terminus extending into the inter-mitochondrial space. This contrasts with Fzo1 and *Tb*MfnL, which are proposed to have a U-shaped structure. Therefore, we have indicated this as TM? in the figure. Structure predictions were performed using PSIPRED.[32] More details and sequence alignment are shown in Figures S1 and S2.

(B) Domain organization of several identified proteins from various organisms. MTS, predicted mitochondrial targeting signal; CC, coiled-coil region; green box, GTPase domain with the four GTP-binding motifs in yellow; TM, transmembrane span; structure predictions were performed using PSIPRED. More details and sequence alignment are shown in Figure S2 and Table S1. *Tb*MfnL, *Trypanosoma brucei* (VEuPathDB: Tb927.7.2410); *Eg*MfnL, *Euglena gracilis* (EukProt V3: EP00667_Euglena_gracilis_P007067); *Dp*MfnL, *Diplonema papillatum* (GenBank: KAJ9468802.1); *Pg*MfnL, *Polarella glacialis* (GenBank: CAE8737761.1); *Ah*MfnL, *Achlya hypogyna* (GenBank: OQR970001); *Ct*MfnL, *Chaetoceros tenuissimus* (GenBank: GFH50037.1); *Hf*MfnL, *Hondaea fermentalgiana* (GenBank: GBG23909.1); *Cht*MfnL, *Chrysochromulina tobinii* (GenBank: KOO35358.1); *Pb*MfnL, *Planctomycetaceae bacterium* (GenBank: MBV8881356.1); *Ps*MfnL, *Pedosphaera* sp. (GenBank: MCH2381658.1); *Rc*MfnL, *Rubrimonas cliftonensis* (GenBank: WP_093253540.1); *Gp*MfnL, *Gammaproteobacteria* bacterium (GenBank: RTZ59088.1); *Mb*MfnL, *Myxococcales* bacterium (GenBank: MCA9558847.1); *Ld*MfnL, *Lentisphaerae* bacterium (GenBank: NLB69313.1); *Kb*MfnL, *Kiritimatiellae* bacterium (GenBank: MBO7223041.1). The accession number for *Euglena longa* was obtained from Eukprot V3 website.

(C) Maximum likelihood phylogenetic tree of eukaryotic and prokaryotic DSPs. The tree was reconstructed using the LG+C60+G4 model of sequence evolution. Ultrafast bootstrap support values are shown on each branch. Taxa are colored according to their taxonomic affiliation. Groups of sequences belonging to the same phylum are collapsed (see also Figure S3 for the complete tree).

(HGT) from bacterial donors. By contrast, the anomalous relationships among eukaryotic taxa observed within the main eukaryotic clade were more difficult to explain, although multiple gene duplications and losses appeared to have played a role in shaping the current distribution of this gene in eukaryotes. The class Diplonemea provided evidence for this hypothesis, with two highly supported (100% UFBS) groups of sequences of the same genera (*Diplonema*, *Lacrimia*, and *Rhynchopus*) branching paraphyletically at the base of a large clade of dinoflagellate (Alveolata) sequences (Figure S3). A small group of sequences containing stramenopile, alveolate, and haptophyte species branched sister to all the other prokaryotic and eukaryotic sequences and most likely represented an ancient paralog of this gene, giving additional evidence for the role of duplication

Please cite this article in press as: Morel et al., A new member of the dynamin superfamily modulates mitochondrial membrane branching in *Trypanosoma brucei*, Current Biology (2025), https://doi.org/10.1016/j.cub.2025.02.033



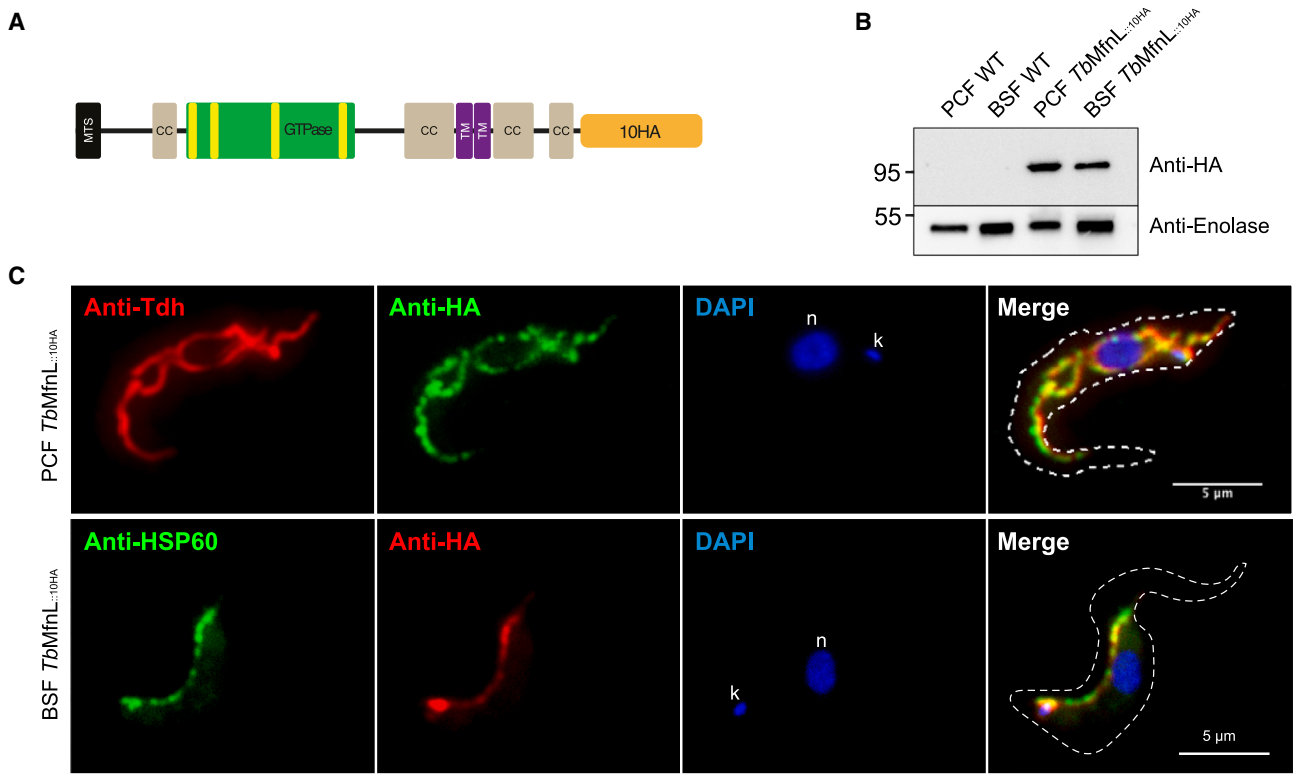


**Figure 2. Subcellular localization of *Tb*MfnL**

(A) Schematic representation of *Tb*MfnL endogenously tagged at its C terminus extremity with 10xHA. Only one of the two alleles is tagged.

(B) Western blotting of whole-cell extracts ($5 \times 10^6$ cells) of *T. brucei* procyclic form (PCF) or bloodstream form (BSF) wild-type cells and PCF or BSF cells expressing *Tb*MfnL$_{::10HA}$ revealed with an anti-HA antibody. It should be noted that Enolase used as a loading control is about 3–4 times more expressed in BSF than in PCF, according to Hannaert et al.[37]

(C) Subcellular localization of *Tb*MfnL$_{::10HA}$ in PCF and BSF. Colocalization of *Tb*MfnL$_{::10HA}$ (anti-HA antibody) with matrix mitochondrial Tdh for PCF (anti-Tdh) and mitochondrial HSP60 for BSF (anti-HSP60) was analyzed by standard immunofluorescence. n, nucleus; k, kinetoplast. The scale bar represents 5 µm.

in the evolution of this gene. Furthermore, it is very likely that HGT between different eukaryotic groups also occurred, as in the case of the dinoflagellate sequences cited above, which appear to have acquired this gene from euglenozoan donors, and in the case of the haptophyte and cryptophyte sequences that branched within the large group of stramenopile sequences.

Given the specific architecture of this DSP, its large phylogenetic distance to other previously known protein families, and its wide and distinct taxonomic representation in prokaryotes and eukaryotes—but its absence in animals and plants—strongly indicate that it represents a novel DSP associated with membrane dynamics.

## *Tb*MfnL is localized in the mitochondrion

To determine the subcellular localization of *Tb*MfnL (VEuPathDB: Tb927.7.2410), we added a 10xHA tag at the C-terminal extremity of the endogenous *Tb*MfnL (*Tb*MfnL$_{::10HA}$) in both PCF and BSF trypanosomes (Figure 2A). C-terminal tagging was used to avoid disruption of the potential N-terminal MTS. Western blot analysis with anti-HA antibody showed that *Tb*MfnL$_{::10HA}$ is about 2-fold more expressed in PCF than in BSF, which is in agreement with the data obtained through SILAC and transcriptomic analysis for this protein (Figure 2B).[33,34] The localization of the *Tb*MfnL protein was studied in PCF by immunofluorescence using threonine dehydrogenase (Tdh[35]) as a mitochondrial matrix marker (Figure 2C). *Tb*MfnL$_{::10HA}$ and Tdh clearly colocalized in the mitochondrial compartment, but *Tb*MfnL depicted a less homogeneous mitochondrial distribution (Figure 2C). Unfortunately, we could not use the anti-Tdh immune serum for immunofluorescence analysis on BSF. Consequently, we performed a labeling of the mitochondria with an anti-HSP60 (mitochondrial maker). Like observed in PCF, *Tb*MfnL$_{::10HA}$ and HSP60 colocalized in the mitochondrial compartment (Figure 2C). The presence of a N-terminal targeting sequence and its localization by fluorescence microscopy demonstrated that *Tb*MfnL is a mitochondrial protein. These data are consistent with the mitochondrial localization of the C-terminal GFP-tagged *Tb*MfnL reported by the TrypTag database (cellular localization of trypanosome proteins).[36] Of note, the N-terminal GFP-tagged *Tb*MfnL exhibited a cytoplasmic localization in TrypTag database,[36] likely due to masking of the MTS pre-sequence.

## Inactivation and silencing of *Tb*MfnL do not alter mitochondrial shape

Live microscopy of yeasts and cultured mammalian cells has revealed that mitochondrial morphology is continuously remodeled by antagonistic fission and fusion reactions.[16,38] Under normal conditions, the fusion/fission balance is established in

Please cite this article in press as: Morel et al., A new member of the dynamin superfamily modulates mitochondrial membrane branching in *Trypanosoma brucei*, Current Biology (2025), https://doi.org/10.1016/j.cub.2025.02.033



CellPress
OPEN ACCESS

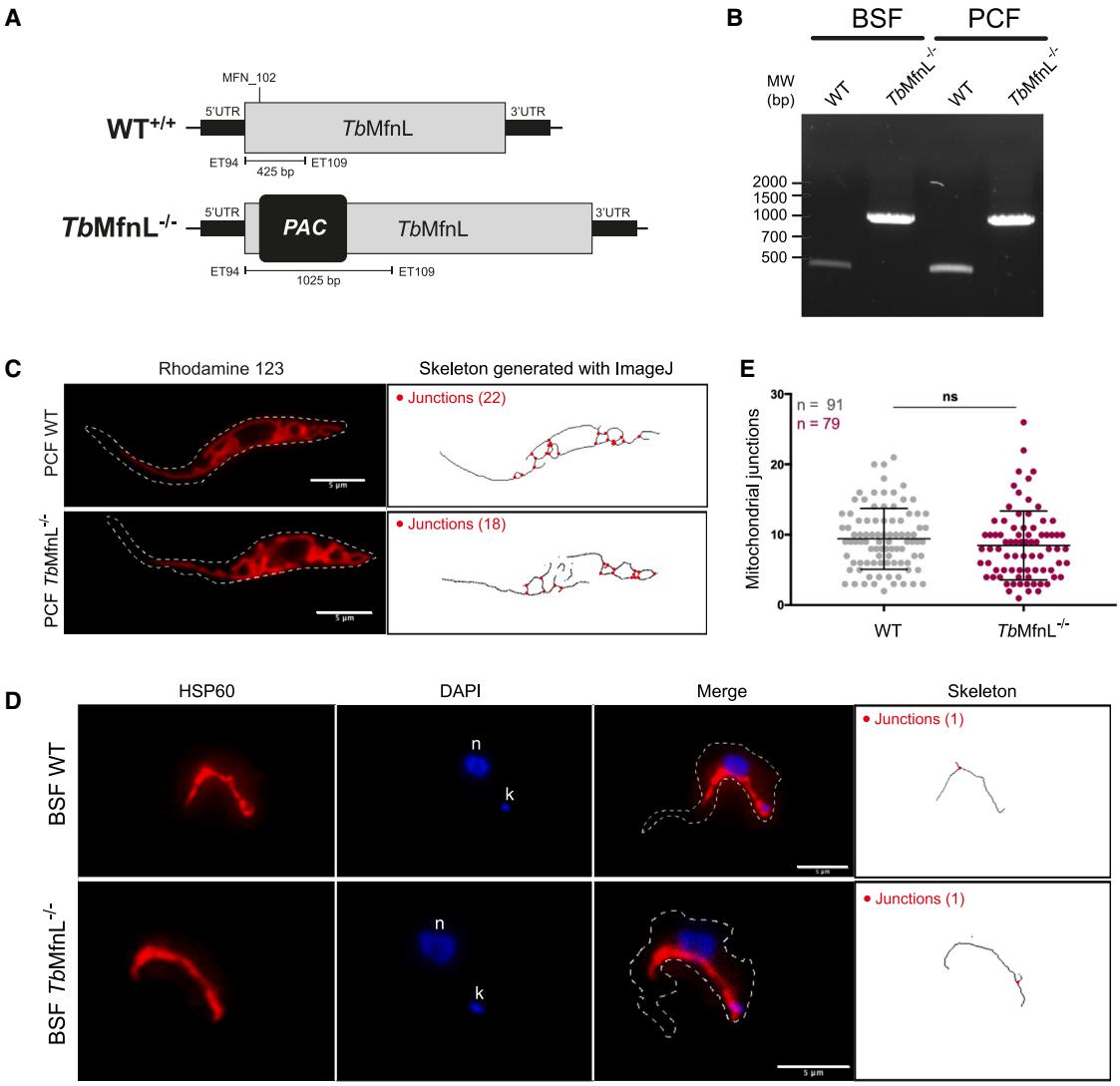


**Figure 3. Inactivation of the *Tb*MfnL gene**

(A) Schematic representation of *Tb*MfnL inactivation by insertion of the puromycine resistant marker (PAC). See also Figures S4–S7.

(B) PCR confirmation of *Tb*MfnL gene inactivation on both alleles in bloodstream form (BSF) and PCF.

(C) The mitochondrial shape of living parental (WT) and *Tb*MfnL$^{-/-}$ PCF cells (right) was designed by an ImageJ macro (mitochondrial junctions) from rhodamine 123 staining (left).

(D) Antibody directed against HSP60 was used to label and visualized mitochondrial shape in BSF cells. Top: BSF parental cell (WT). Bottom: BSF *Tb*MfnL$^{-/-}$ cell. n, nucleus; k, kinetoplast.

(E) Corresponding mitochondrial junctions' quantification. Small red circles in the skeleton image indicate the junctions where three tubules converge. The scale bar represents 5 μm. Statistic: t test (ns, $p \geq 0.05$; *$p < 0.05$, **$p < 0.01$, ***$p < 0.001$).

favor of fusion, and the mitochondria appear filamentous. Inhibition of fusion leads to mitochondrial fragmentation by ongoing fission,[16] and conversely, enhancing fusion leads to hyperfused mitochondria with increased branching and interconnection.[12]

To investigate the role of *Tb*MfnL, we first inactivated the *Tb*MfnL gene by CRISPR-Cas9.[39] Both *Tb*MfnL alleles were inactivated by the integration of a puromycin resistance marker cassette into both PCF and BSF cloned cells (Figure 3A). Cloned parasites were analyzed by PCR to select cell lines carrying puromycin resistance gene insertions in both *Tb*MfnL alleles (*Tb*MfnL$^{-/-}$) (Figure 3B). No significant impact on cell growth was observed in these PCF and BSF null mutants over a period of 7 days compared with parental cells (Figure S4), and no significant difference in the structure of the *Tb*MfnL$^{-/-}$ mitochondrion was observed by staining mitochondrion with rhodamine-123 or immunofluorescence analyses with the anti-HSP60 immune serum in both PCF and BSF mutant cell lines, respectively (Figures 3C and 3D). To confirm that the CRISPR-Cas9 strategy leads to *Tb*MfnL gene inactivation, we repeated this process in a strain endotagged with a C-terminal 3xTy1 tag in order to follow the expression of the protein by western blot (Figures S5A–S5D) upon insertion of the puromycin resistance gene as above

Please cite this article in press as: Morel et al., A new member of the dynamin superfamily modulates mitochondrial membrane branching in *Trypanosoma brucei*, Current Biology (2025), https://doi.org/10.1016/j.cub.2025.02.033



(Figures S5E–S5G) and deletion of part of the *Tb*MfnL gene (Figures S5H–S5J), as above. In both cases, the protein was not detected in the inactivated clones, and no modification of the mitochondrial structure was observed (Figures S5G and S5J).

In order to detect and quantify discrete modifications of the mitochondrial shape that may escape detection upon qualitative visual analysis, we developed an ImageJ macro (Methods S1) for automatic quantification of mitochondrial junctions from fluorescence images (Figures 3C–3E). This enabled us to determine that the number of mitochondrial junctions was reduced in *Tb*MfnL$^{-/-}$ cells compared with the parental PCF cells (8.5 ± 4.9 vs. 9.4 ± 4.3), although this difference was not statistically significant. This finding supports the qualitative analysis of the microscopy images (Figure 3C). The mitochondrial and cristae structures were also examined by transmission electron microscopy (TEM) in *Tb*MfnL$^{-/-}$ PCF cells cultured with either proline or glucose as the sole carbon source. Under these conditions, no significant alterations in mitochondrial or cristae structure were observed, nor were there any noticeable effects on the growth of the mutant cells (Figure S6).

These findings regarding the consequences of *Tb*MfnL inactivation in PCF and BSF are not in line with a previous report describing a highly fenestrated mitochondrial network consecutive to a partial but significant inhibition (70%) of *Tb*MfnL expression by RNAi in BSF.[30] To exclude that the divergence arose from the different inactivation and silencing strategies, we conditionally downregulated expression of *Tb*MfnL using a stem-loop RNAi construct. This approach led to a significant reduction (~70%) of the expression of endogenously tagged *Tb*MfnL$_{::10HA}$ in PCF (as observed in BSF[30]), but this was not paralleled by a modification of mitochondrial shape (Figures S7A–S7C). Since mitochondrial fenestration upon *Tb*MfnL silencing was observed in BSF,[30] we decided to repeat the experiment using the same strain (*T. brucei* 427 BSF), the same RNAi system (p2T7-177), and the same sequence used for downregulation.[30] As previously reported,[30] we observed a significant reduction of *T*bMfnL expression (~80% after 4 days) of the endogenously tagged *Tb*MfnL$_{::3HA}$ in BSF (Figures S7D–S7F) that was not accompanied by mitochondrial shape modifications (Figure S7G). In our hands, neither inactivation nor silencing of *Tb*MfnL alters mitochondrial morphology or induces a fenestration phenotype.

### *Tb*MfnL overexpression increases mitochondrial branching

We also investigated the possible role of *Tb*MfnL by conditionally overexpressing a C-terminally tagged (3xTy1) *Tb*MfnL in PCF ($^{oe}$*Tb*MfnL$_{::3Ty1}$; Figure 4A). Expression was confirmed by western blot analysis after 3–5 days of tetracycline induction (Figure 4B). No significant impact on cell growth was observed over a period of 7 days compared with parental cells (Figure S4). Rhodamine-123 staining showed that the parental and non-induced $^{oe}$*Tb*MfnL$_{::3Ty1}$ cell lines harbor the expected reticulated mitochondrial structure, while the mitochondrion appears significantly more reticulated and branched in the tetracycline-induced $^{oe}$*Tb*MfnL$_{::3Ty1}$ cells (Figures 4C and S8). After 5 days of induction, the average number of mitochondrial junctions, quantified with the ImageJ macro, appeared more than 2 times higher in induced $^{oe}$*Tb*MfnL$_{::3Ty1}$ cells compared with non-induced or parental cells (Figure 4D). In order to estimate the level of *Tb*MfnL overexpression achieved in *T. brucei* PCF, we overexpressed *Tb*MfnL$_{::3Ty1}$ in the *Tb*MfnL$_{::3Ty1}$ background, in which the endogenous *Tb*MfnL alleles were 3Ty1-tagged (clone 2A11; Figures S5A–S5D). Western blot analysis with the anti-Ty1 antibodies revealed that expression of *Tb*MfnL$_{::3Ty1}$ is 5.5 times increased in the resulting tetracycline-induced *Tb*MfnL$_{::3Ty1}$/$^{oe}$*Tb*MfnL$_{::3Ty1}$ compared with the parental *Tb*MfnL$_{::3Ty1}$ clone, which only expressed the endogenously tagged *Tb*MfnL$_{::3Ty1}$ (Figure S8A). Overexpression of *Tb*MfnL$_{::3Ty1}$ once again leads to alterations in mitochondrial morphology. It is also noteworthy that the expression of *Tb*MfnL without the C-terminal 3Ty1 tag induced the same phenotype as the tagged *Tb*MfnL, confirming that the phenotype is not due to the use of a C-terminal tag (Figures S8A and S8B). These data clearly demonstrated that overexpression of *Tb*MfnL stimulates inter-mitochondrial connections.

To characterize further inter-mitochondrial branching with higher resolution we used serial block face scanning electron microscopy (SBF-SEM), an approach allowing us to characterize the overall structure of membranes and organelles within the entire cell volume.[18] With this approach, hundreds of images are collected to perform a 3D reconstruction of the whole cell, as well as spatial organization of the individual organelles within the cell. Four to five parental and $^{oe}$*Tb*MfnL$_{::3Ty1}$ PCF cells were reconstructed in 3D, with a particular emphasis on the mitochondrion, the nucleus, the flagellar pocket, and the cell outline. We have not been able to correctly identify the kDNA on the electron microscopy images. However, since kDNA is in close contact with the flagellar pocket, we have assumed its position. Other organelles (glycosomes, acidocalcisomes, Golgi, flagellum, etc.) are not represented either in order to not overload the 3D representation. As expected, the parental PCF cells showed a reticulated mitochondrion along the whole cell (Figure 4E), a rather central nucleus, and the flagellar pocket on the posterior side. The length of the parental and $^{oe}$*Tb*MfnL$_{::3Ty1}$ cells varied between 20.4 ± 3.3 and 23 ± 4.7 μm, respectively. As observed by fluorescence microscopy, $^{oe}$*Tb*MfnL$_{::3Ty1}$ mitochondrion showed more reticulation (Figure 4E). Unexpectedly, in some cells this reticulation was even more prominent at the edges of the flagellar pocket, where the kDNA is located, as illustrated in Figure 4E, an observation that we had not identified by immunofluorescence microscopy approaches. This hyper-reticulated structure (leaving a few gaps in the mitochondrion) formed a globular structure and probably encapsulated the kDNA (Figure 4E). This structure, called the kDNA pocket, has already been described in BSF, where kDNA replicates[20] but is even more prominent in the $^{oe}$*Tb*MfnL$_{::3Ty1}$ cells. We determined that the mitochondrial volume in PCF cells (4.9 ± 1 μm$^3$; Figure 4F) aligns with previous reports (2.5–3 μm$^3$; Bílý et al.[2]) and as expected, is nearly twice that of BSF cells (1.1–3 μm$^3$).[18,20] As anticipated, the mitochondrial volume in $^{oe}$*TbMfnL$_{::3Ty1}$* cells is nearly doubled compared with parental cells (8.3 ± 1.9 μm$^3$; Figure 4F). Additionally, TEM analysis of the mitochondrial and cristae structures in $^{oe}$*Tb*MfnL$_{::3Ty1}$ cells cultured with either proline or glucose as the sole carbon source revealed no significant alterations (Figure S6).

We also investigated the effect of *Tb*MfnL expression in the BSF trypanosomes, where the mitochondrial compartment is smaller

Please cite this article in press as: Morel et al., A new member of the dynamin superfamily modulates mitochondrial membrane branching in *Trypanosoma brucei*, Current Biology (2025), https://doi.org/10.1016/j.cub.2025.02.033



CellPress
OPEN ACCESS

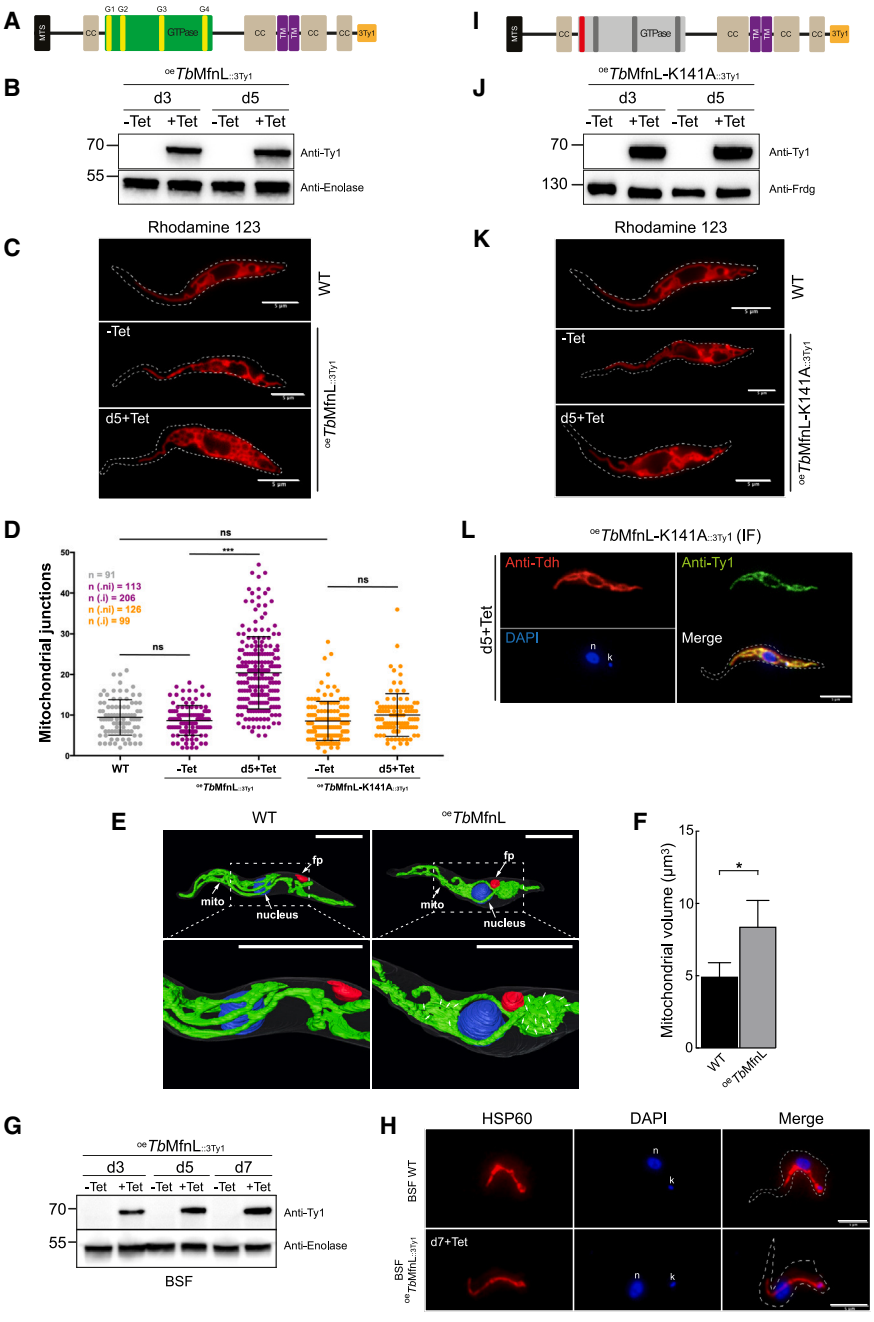


**Figure 4. Overexpression of *Tb*MfnL and GTPase mutant**

(A) Schematic representation of the over-expressing *Tb*MfnL protein tagged with 3Ty1 peptide at the C terminus of the protein ($^{oe}$*Tb*MfnL$_{::3Ty1}$).

(B) Western blotting of whole-cell extracts of *T. brucei* PCF cells overexpressing *Tb*MfnL$_{::3Ty1}$. Non-induced (−Tet) and induced (+Tet) cells after 3–5 days were revealed with an anti-Ty1 antibody. Antibody directed against Enolase protein was used as loading control.

(C) Mitochondrial structure analysis using rhodamine 123 staining on living cells. Mitochondrial structure of PCF parental (WT) and PCF $^{oe}$*Tb*MfnL$_{::3Ty1}$ cells before (−Tet) and 5 days after (+Tet) tetracycline induction. See also Figures S4–S6 and S8–S10.

(D) Quantification of mitochondrial junctions' number using rhodamine 123 microscopy images. Mitochondrial junctions number: WT, 9.4 ± 4.3; −Tet $^{oe}$*Tb*MfnL$_{::3Ty1}$, 8.7 ± 3.6; +Tet $^{oe}$*Tb*MfnL$_{::3Ty1}$, 20.4 ± 8.9; −Tet $^{oe}$*Tb*MfnL-K141A$_{::3Ty1}$, 8.6 ± 4.8; +Tet $^{oe}$*Tb*MfnL-K141A$_{::3Ty1}$, 10 ± 5.2. Statistic: t test (ns, $p \geq 0.05$; *$p < 0.05$, **$p < 0.01$, ***$p < 0.001$).

(E) Surface rendering of segmented PCF using SBF-SEM. Surface rendering of segmented PCF WT and $^{oe}$*Tb*MfnL cells, with $^{e}$*Tb*MfnL induced by tetracycline for 5 days, showing the cell body (transparent), nucleus (blue), mitochondrion (green), and flagellar pocket (red). 5 WT and 4 $^{oe}$*Tb*MfnL cells were analyzed. A magnified view of the upper images, enclosed in a box, was shown. Small white arrows mark the mitochondria-free areas within the mitochondrial network.

(F) Determination of mitochondrial volume (µm$^3$) in both WT and $^{oe}$*Tb*MfnL cells: WT, 4.9 ± 1; $^{oe}$*Tb*MfnL, 8.3 ± 1.9. Statistic: t test (ns, $p \geq 0.05$; *$p < 0.05$, **$p < 0.01$, ***$p < 0.001$).

(G) Western blotting of whole-cell extracts of *T. brucei* bloodstream form (BSF) overexpressing *Tb*MfnL$_{::3Ty1}$ cells. Non-induced (−Tet) and induced (+Tet) cells after 3–7 days were revealed with an anti-Ty1 antibody. Antibody directed against Enolase protein was used as loading control.

(H) Subcellular localization of $^{oe}$*Tb*MfnL$_{::3Ty1}$ in BSF by immunofluorescence. Antibody directed against HSP60 was used to label and visualize mitochondrial shape in parental (WT) and *Tb*MfnL$_{::3Ty1}$ overexpressing cells. n, nucleus; k, kinetoplast. The scale bar represents 5 µm.

(I) Schematic representation of the over-expressing *Tb*MfnL-K141A$_{::3Ty1}$ mutant protein tagged with 3Ty1 peptide at the C terminus of the protein ($^{oe}$*Tb*MfnL-K141A$_{::3Ty1}$).

(J) Western blotting of whole-cell extracts of *T. brucei* PCF overexpressing *Tb*MfnL-K141A$_{::3Ty1}$ cells; (−Tet) non-induced and (+Tet) induced cells for 3 or 5 days. Antibody directed against glycosomal fumarate reductase protein (Frdg) was used as loading control.

(K) Mitochondrial structure analysis using rhodamine 123 staining on living cells. Mitochondrial structure of PCF parental (WT) and PCF $^{oe}$*Tb*MfnL-K141A$_{::3Ty1}$ cells before (−Tet) and 5 days after (+Tet) tetracycline induction. The scale bar represents 5 µm. See also Figures S5 and S8–S10.

(L) Submitochondrial localization of $^{oe}$*Tb*MfnL-K141A$_{::3Ty1}$ in PCF by immunofluorescence. Colocalization of $^{oe}$*Tb*MfnL-K141A$_{::3Ty1}$ (anti-Ty1) with matrix mitochondrial threonine dehydrogenase (anti-Tdh) was analyzed by standard immunofluorescence after 5 days of induction (day 5 + Tet). n, nucleus; k, kinetoplast.

and composed of a shorter and poorly interconnected mitochondrion. Expression of $^{oe}$*Tb*MfnL$_{::3Ty1}$ was confirmed by western blot (Figure 4G), but unlike in PCF, the mitochondrial structure (labeled here with mitochondrial HSP60) was not altered, remaining tubular like in the parental cells (Figure 4H). Induction over a longer period (up to 21 days) did not show mitochondrial alterations.

Please cite this article in press as: Morel et al., A new member of the dynamin superfamily modulates mitochondrial membrane branching in *Trypanosoma brucei*, Current Biology (2025), https://doi.org/10.1016/j.cub.2025.02.033



### *Tb*MfnL overexpression increases mitochondrial branching in a GTPase-dependent manner

All dynamin-like proteins possess a GTP-binding domain with highly conserved G1-G4 motifs. They can be inactivated by mutations in the G1 motif that lower the efficiency of GTP binding and hydrolysis. To determine whether *Tb*MfnL activity requires a functional GTPase domain, the key lysine 141 in the highly conserved G1 motif was converted to alanine (K141A), according to previously characterized GTP-binding domains from other organisms.[40–42] The K141A mutation was introduced into the *Tb*MfnL$_{::3Ty1}$ sequence, which was overexpressed in the PCF $^{oe}$*Tb*MfnL-K141A$_{::3Ty1}$ (Figure 4I) and *Tb*MfnL$_{::3Ty1}$ PCF backgrounds (*Tb*MfnL$_{::3Ty1}$/$^{oe}$*Tb*MfnL-K141A$_{::3Ty1}$; Figure S8). Expression of *Tb*MfnL-K141A$_{::3Ty1}$ was confirmed by western blot analyses after 3–5 days of tetracycline induction in the $^{oe}$*Tb*MfnL-K141A$_{::3Ty1}$ cell line (Figure 4J), and its overexpression was estimated as 3-fold in the *Tb*MfnL$_{::3Ty1}$/$^{oe}$*Tb*MfnL-K141A$_{::3Ty1}$ mutant compared with the parental *Tb*MfnL$_{::3Ty1}$ clone (Figure S8A). *Tb*MfnL-K141A$_{::3Ty1}$ localized to the mitochondria (Figure 4L), as expected, but did not alter mitochondrial shape (Figures 4K, 4L, and S8) nor the number of mitochondrial junctions (Figure 4D). To exclude the possibility that concentration-dependent effects (due to the 2-fold lower expression of *Tb*MfnL-K141A$_{::3Ty1}$ compared with the parental *Tb*MfnL$_{::3Ty1}$) might prevent K141A from inducing membrane branching, rather than its inactivated GTPase activity, we equalized the expression levels of wild-type *Tb*MfnL$_{::3Ty1}$ and mutant *Tb*MfnL-K141A$_{::3Ty1}$. The tetracycline concentration used for *Tb*MfnL$_{::3Ty1}$ expression was reduced from 1 to 0.05 μg/mL. Under these conditions, both variants displayed comparable expression levels at 3 and 5 days (Figure S9A); however, hyper-reticulation was observed exclusively in cells overexpressing *Tb*MfnL$_{::3Ty1}$ (Figure S9B). This clearly demonstrates that *Tb*MfnL is a dynamin-related protein that relies on a functional GTPase domain to modulate mitochondrial branching in trypanosomes.

The mitochondrial localization of $^{oe}$*Tb*MfnL$_{::3Ty1}$ and $^{oe}$*Tb*MfnL-K141A$_{::3Ty1}$ was also confirmed by electron microscopy and immunogold labeling using an anti-Ty1 antibody. After induction and immunogold labeling, both proteins are clearly localized in the mitochondrion (Figures S10A and S10B, c and d) as compared with controls with non-induced cells (Figures S10A and S10B, a and b) and confirmed by gold-particle quantification (Figure S10C).

### Submitochondrial localization of *Tb*MfnL

Immunofluorescence analyses showed that $^{oe}$*Tb*MfnL$_{::3Ty1}$ co-localized with Tdh (Figure 5A), as previously described for the endogenously tagged *Tb*MfnL$_{::10HA}$ (Figure 2C). To increase the resolution of *Tb*MfnL localization, we performed ultrastructure expansion microscopy (UExM), which increases the size of a sample while preserving its ultrastructure.[43–45] Using this approach, we showed that both $^{oe}$*Tb*MfnL$_{::3Ty1}$ (Figure 5B) and the endogenous *Tb*MfnL$_{::10HA}$ (Figure 5C) displayed mitochondrial localization with punctate, non-homogeneous distribution. This localization pattern differed from that of the matrix marker (Tdh) and may be attributed to predicted membrane integration, as suggested by the predicted TMs.

### Mitochondrial targeting and membrane anchoring of *Tb*MfnL

To investigate the mechanisms ensuring mitochondrial targeting of *Tb*MfnL, we first addressed the two domains that may determine *Tb*MfnL localization: (1) the N-terminal MTS, which may facilitate targeting to the inner membrane, intermembrane space, and matrix localization, and (2) the C-proximal/terminal TMs, which could mediate membrane anchoring. To investigate their capacity to target proteins to mitochondria, we fused the MTS domain, or the two transmembrane domains of *Tb*MfnL, to GFP. Fusion of the MTS at the N terminus of GFP ($_{MTS::}$GFP) fully targeted GFP to the mitochondria (Figure 6A). Interestingly, western blot analyses showed that $_{MTS::}$GFP and cytosolic GFP (cGFP) have the same apparent size (Figure 6B), suggesting that the predicted MTS (Figure S1) was indeed cleaved by matrix processing peptidase upon import of $_{MTS::}$GFP across the inner membrane. By contrast, western blot analyses showed that the addition of the two C-proximal TMs at the C-terminal extremity of GFP (GFP$_{::TM}$) induces a size shift (Figure 6B). Immunofluorescence analyses revealed that GFP$_{::TM}$ was not targeted to the mitochondrion or cytosol but instead to other distinct structures (Figure 6A). However, it is important to note that this localization could simply represent unspecific membrane-targeting by hydrophobic TMs. This inability of *Tb*MfnL TMs to mediate mitochondrial targeting indicates that they differ from the TMs of other Mfns, which are responsible for mitochondrial outer membrane localization.[46]

To confirm the role and relevance of these domains on *Tb*MfnL localization and function, we overexpressed 3Ty1-tagged *Tb*MfnL-mutants without MTS ($^{oe}$*Tb*MfnL-ΔMTS$_{::3Ty1}$) or without TMs ($^{oe}$*Tb*MfnL-ΔTM$_{::3Ty1}$) in PCF trypanosomes (Figures 6D and 6G). Tetracycline-induced overexpression of both recombinant *Tb*MfnL was confirmed by western blot, 3–5 days after induction (Figures 6E, 6H, and S8). No significant impact on cell growth was observed over a period of 7 days compared with parental cells (Figure S4). In contrast to $^{oe}$*Tb*MfnL$_{::3Ty1}$, $^{oe}$*Tb*MfnL-ΔMTS$_{::3Ty1}$ did not colocalize with Tdh, revealing that the N-terminal MTS is indeed required for proper mitochondrial targeting of *Tb*MfnL (Figure 6F). The MTS is therefore essential for the correct mitochondrial localization of *Tb*MfnL. In addition, overexpression of $^{oe}$*Tb*MfnL-ΔMTS$_{::3Ty1}$ did not alter the mitochondrial structure, indicating that its proper, MTS-mediated, mitochondrial localization is essential for *Tb*MfnL function (Figures 6F and S8). Overexpression of a *Tb*MfnL truncated version missing the C-proximal TMs ($^{oe}$*Tb*MfnL-ΔTM$_{::3Ty1}$, Figures 6G, 6H, and S8) did not affect its mitochondrial localization (Figure 6I), which confirms that the N-terminal MTS sequence was sufficient for mitochondrial targeting of *Tb*MfnL. However, in contrast to full-length *Tb*MfnL (Figures 4C, 5A, and 5B), *Tb*MfnL lacking TMs did not induce a modification of the mitochondrial shape (Figures 6I and S8), demonstrating that the transmembrane domains are required for proper function. Altogether, our data showed that *Tb*MfnL is targeted to the mitochondrion via an N-terminal MTS and that C-proximal TMs are required for the cellular function of *Tb*MfnL.

Finally, we investigated the precise localization of *Tb*MfnL$_{::3Ty1}$ and its variants (*Tb*MfnL-ΔTM$_{::3Ty1}$ and *Tb*MfnL-ΔMTS$_{::3Ty1}$) in the clone 2A11, where the endogenous *Tb*MfnL alleles were tagged with 3Ty1 (Figures S5A–S5D). This was achieved using

Please cite this article in press as: Morel et al., A new member of the dynamin superfamily modulates mitochondrial membrane branching in *Trypanosoma brucei*, Current Biology (2025), https://doi.org/10.1016/j.cub.2025.02.033



CellPress
OPEN ACCESS

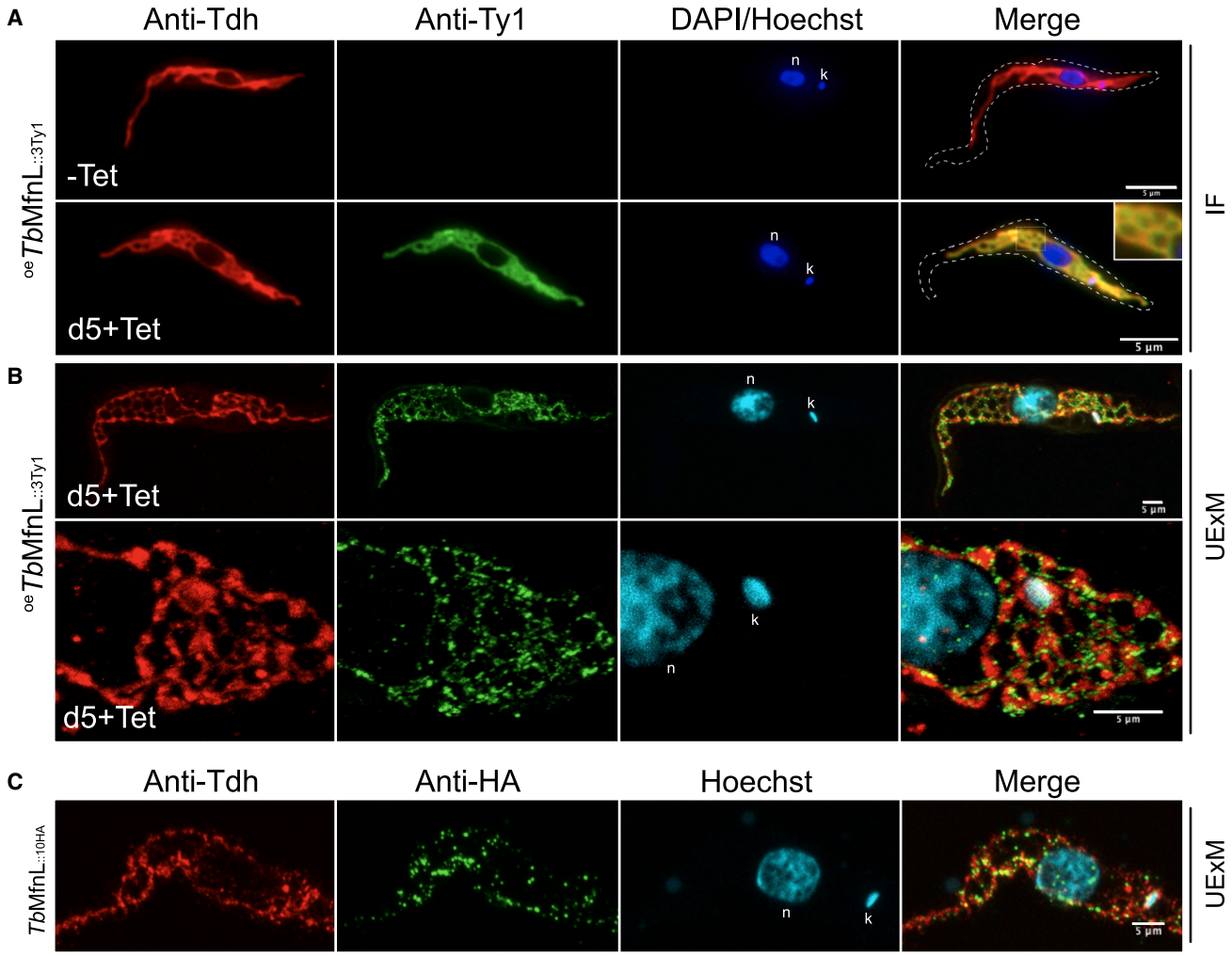


**Figure 5. Submitochondrial localization of *Tb*MfnL**

(A and B) Subcellular localization of $^{oe}$*Tb*MfnL$_{::3Ty1}$ in PCF by immunofluorescence and ultra expansion microscopy (UExM). Colocalization of $^{oe}$*Tb*MfnL$_{::3Ty1}$ (anti-Ty1) with matrix mitochondrial threonine dehydrogenase (anti-Tdh) was analyzed by standard immunofluorescence (A) and by UExM with an expansion factor of ~4.4 (B), after 5 days of induction (day 5 + Tet).

(C) Subcellular localization of $^{oe}$*Tb*MfnL$_{::10HA}$ in PCF analyzed by UExM. n, nucleus; k, kinetoplast. The scale bar represents 5 µm.

a protease protection assay, a method previously used to determine the submitochondrial localization of various mitochondrial proteins in trypanosomes.[47,48] Mitochondria are enriched by differential centrifugation, converted into mitoplasts by digitonin-mediated permeabilization of the outer membrane, and finally incubated with Proteinase K in the presence or absence of Triton X-100 to permeabilize the inner membrane.

Western blot analysis revealed that the cytosolic protein Enolase was almost entirely recovered in the supernatant, confirming that the generation of mitoplasts had effectively released cytosolic components (Figure 7A). By contrast, the *Tb*MfnL$_{::3Ty1}$ protein and its variants exhibited fractionation patterns consistent with those of mitochondrial proteins, such as Atom40, Prohibitin, and Tdh, which serve as markers for the outer mitochondrial membrane, inner mitochondrial membrane (facing the intermembrane space), and mitochondrial matrix, respectively (Figures 7A and 7C). Proteinase K treatment of mitoplasts led to the near-complete digestion of outer membrane Atom40, intermembrane space Prohibitin (bound to the inner membrane), and *Tb*MfnL-ΔMTS$_{::3Ty1}$, which is no longer targeted to the mitochondrion and thus unprotected. By contrast, the size and levels of *Tb*MfnL$_{::3Ty1}$, *Tb*MfnL-ΔTM$_{::3Ty1}$, and Tdh remained unaffected, indicating protease protection by the inner membrane. The intact state of Tdh further confirmed the integrity of the mitochondrial inner membrane and the reliability of the assay (Figures 7A and 7C). Digestion of the outer mitochondrial membrane-embedded β-barrel protein Atom40 and inter-mitochondrial space Prohibitin, along with the preservation of *Tb*MfnL$_{::3Ty1}$ and *Tb*MfnL-ΔTM$_{::3Ty1}$, suggests that *Tb*MfnL faces the matrix and is protected by the inner membrane. The addition of Triton X-100, which disrupts membrane integrity, exposed matrix proteins to Proteinase K, resulting in the degradation of *Tb*MfnL$_{::3Ty1}$, *Tb*MfnL-ΔTM$_{::3Ty1}$, and Tdh, thereby confirming their localization and orientation on the matrix side (Figures 7A

Please cite this article in press as: Morel et al., A new member of the dynamin superfamily modulates mitochondrial membrane branching in *Trypanosoma brucei*, Current Biology (2025), https://doi.org/10.1016/j.cub.2025.02.033



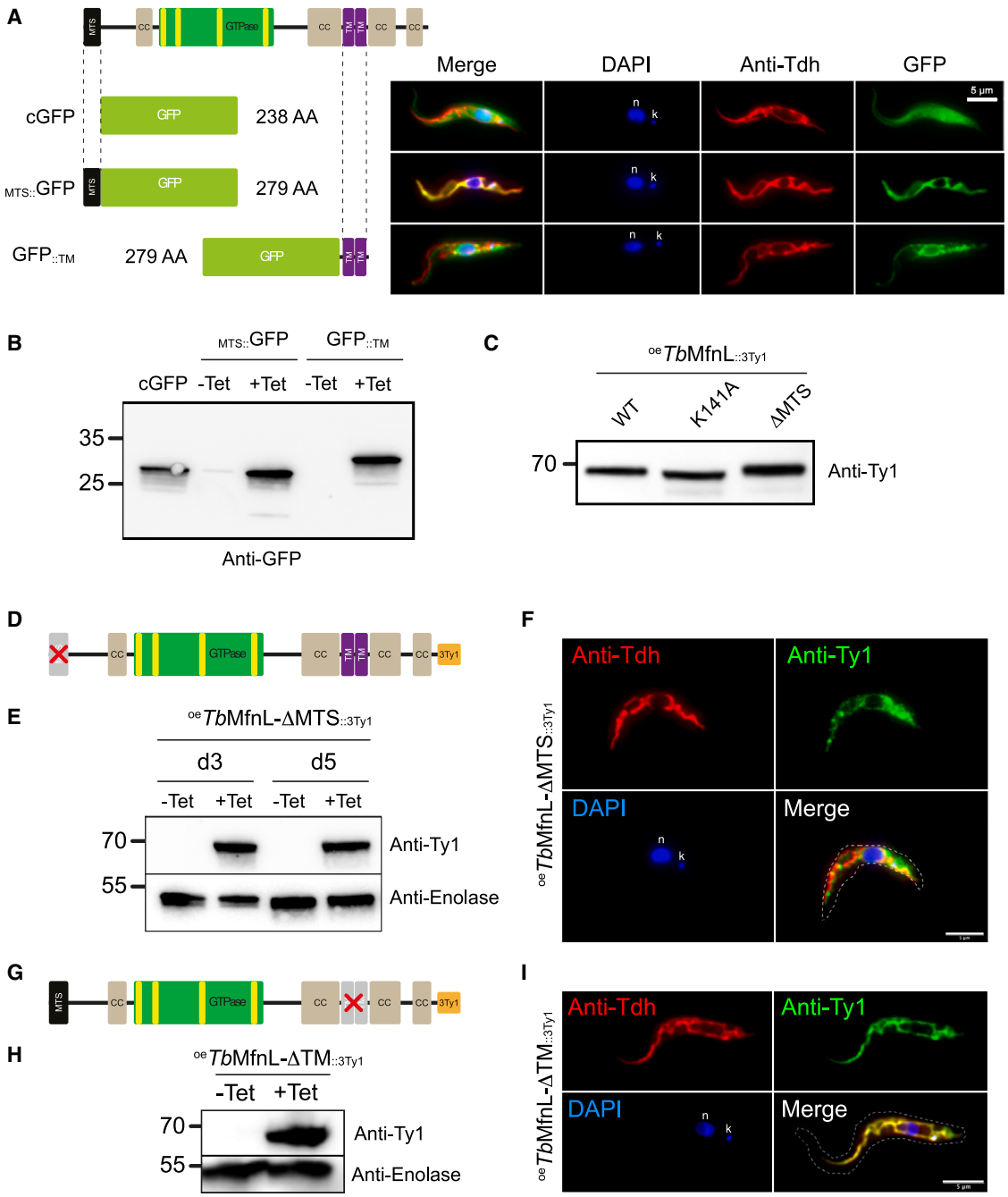


**Figure 6. Role of *Tb*MfnL domains**

(A) Localization of the GFP according to the different tags fused. Colocalization of GFP with the mitochondrial matrix marker threonine dehydrogenase (anti-Tdh) was assessed by standard immunofluorescence after 5 days of tetracycline induction for MTS$_{::GFP}$ and GFP$_{::TM}$. The "c" in cGFP stands for constitutive expression, resulting in the cytosolic localization of GFP. MTS, mitochondrial targeting signal; TMs, transmembrane domains.

(B) Western blot analysis of GFP expression. cGFP, constitutive and cytosolic GFP. Non-induced (−Tet) and induced (+Tet) cells after 5 days.

(C) *Tb*MfnL size analysis by western blot using anti-Ty1 antibody.

(D) Schematic representation of N terminus truncated *Tb*MfnL protein (first 41 amino acids) tagged with 3Ty1 peptide at the C terminus of the protein ($^{oe}$*Tb*MfnL-ΔMTS$_{::3Ty1}$).

(E) Western blotting of whole-cell extracts of *T. brucei* PCF overexpressing *Tb*MfnL-ΔMTS$_{::3Ty1}$ cells; (−Tet) non-induced and (+Tet) induced cells for 3 or 5 days.

(F) Subcellular localization of $^{oe}$*Tb*MfnL-ΔMTS$_{::3Ty1}$ in PCF after 5 days of induction. Colocalization of $^{oe}$*Tb*MfnL-ΔMTS$_{::3Ty1}$ (anti-Ty1) with matrix mitochondrial threonine dehydrogenase (anti-Tdh) analyzed by standard immunofluorescence.

*(legend continued on next page)*

and 7C). It should be noted that western blot revealed a size difference between the full-length *Tb*MfnL$_{::3Ty1}$ and *Tb*MfnL-ΔTM$_{::3Ty1}$. Specifically, we observed two bands: the upper band corresponding to the endogenously tagged protein and the lower band representing the overexpressed *Tb*MfnL-ΔTM$_{::3Ty1}$ protein.

To further investigate the localization of *Tb*MfnL, we separated the membrane and matrix fractions by performing repeated freeze-thaw lysis on mitoplast preparations. The membrane fraction was further divided into integral and peripheral fractions via carbonate extraction. *Tb*MfnL$_{::3Ty1}$ and *Tb*MfnL-ΔTM$_{::3Ty1}$ were analyzed alongside control proteins, Tdh (matrix-localized) and Prohibitin (inner membrane, inter-mitochondrial space oriented). As expected, *Tb*MfnL$_{::3Ty1}$ was exclusively retained in the membrane fraction, whereas *Tb*MfnL-ΔTM$_{::3Ty1}$, lacking its TMs, was released from membrane (Figures 7B and 7C). These data are consistent with a recent analysis of the mitochondrial proteome, which proposed that the *Tb*MfnL protein is located in the inner mitochondrial membrane.[49]

Interestingly, structural predictions of *Tb*MfnL using AlphaFold, supported by a very high pLDDT score, suggest that the two previously identified transmembrane domains form a loop. This loop may act as an anchor within the inner membrane, thereby orienting the protein toward the matrix (Figure 7C), consistent with the findings from Proteinase K assay and carbonate extraction.

## DISCUSSION

Membrane fusion and fission are often controlled by proteins of the DSP.[50,51] These proteins consistently have a GTPase domain and contain domains required for membrane binding and oligomerization. In trypanosomes, only DSPs involved in fission have been characterized, and no fusion proteins similar to those of yeasts and mammals (Mfn and Opa1) have been identified so far. This may suggest that trypanosome mitochondria fuse via a machinery that differs from that characterized in yeasts and mammals. We have identified a novel DSP, named Mfn-like (MfnL), which represents the first characterized DSP from the protozoan parasite *T. brucei* (*Tb*MfnL). We did not establish a direct role in fusion but demonstrated that it is able to increase mitochondrial interconnectivity in a GTPase-dependent manner, as previously reported for fusion factors Mfn/Opa1.[46,52] Interestingly, *Tb*MfnL domain organization and submitochondrial localization differ significantly from that of Mfn and Opa1, suggesting that *Tb*MfnL and possibly other MfnL members mediate and/or enhance membrane branching and interconnection through a different molecular mechanism.

As observed for trypanosomes, many organisms, including plants, lack genes encoding protein similar to known fusion factors. Interestingly, the search for homologous sequences to *Tb*MfnL allowed us to identify close DSP homologs in several eukaryotic phyla lacking Mfn and Opa1. These new DSPs are widely distributed in eukaryotes, which suggests that they represent an ancient protein family. Most of these phyla belong to the Diphoda, which together with the Opimoda are the two major supergroups of eukaryotes based on the most accepted position of the root of the tree of eukaryotes.[53] The only opimodan sequences found were the two amoeba cited above, most likely representing HGTs from bacteria, and the malawimonad *Gefionella okellyi* (Figures 1C and S3). This malawimonad sequence may also reflect an HGT acquisition, in this case from a diphodan ancestor. The taxonomic distribution of this protein and its phylogeny support that it was ancestral at least in Diphoda. However, its presence also in bacteria, with any clear evidence of an HGT-mediated eukaryotic origin of the bacterial sequences, opens the possibility for an even more ancient origin before the diversification of Diphoda and Opimoda, which would imply a massive loss in opimodan taxa except in a few ones such as *Gefionella*. Future analysis of other deep-branching opimodan taxa will help to test this hypothesis. Homologs of *Tb*MfnL were also identified in several bacterial phyla, suggesting the existence in these organisms of a novel machinery involved in membrane shaping and/or remodeling that is different from the one found in yeasts and mammals. While studies of yeast and mammalian DSPs provide information about their functions and structures, little is known about bacterial DSPs, especially their cellular role. Indeed, some bacterial DSPs have been associated with a variety of processes involving membranes *in vivo*, such as a surveillance mechanism for membrane punctures caused by antibiotics and bacteriophages,[54,55] membrane vesicle formation,[56] or cytokinesis by promoting membrane curvature at the septum.[57,58] In addition, studies of the *Bacillus subtilis* DSP DynA have shown that this protein can promote membrane fusion *in vitro*.[59] The mechanism by which the fusion operates is not yet known, but bacterial DSPs are probably recruited to the sites where membrane fusion is needed.[58,60] Interestingly, structural analysis of *Campylobacter jejuni* DLP1/DLP2 proteins allowed us to propose a mechanism explaining how these proteins attach and bind distant and opposing membranes.[61] Unfortunately, the cellular function of *C. jejuni* DLP1/DLP2 is currently unknown. DSPs identified in this study have not yet been characterized, and no information on their localization and function is available. However, among the identified organisms, we found bacteria of the phylum Planctomycetes, which are unusual organisms. Indeed, these bacteria contain a compartmentalized cytosol, separated by an intracytoplasmic membrane,[62] in some cases surrounding the DNA[63] or forming an anammoxosome, a membrane-bound organelle responsible for the production of energy.[64,65] It is then conceivable that the identified protein in Planctomycetes (*Pb*DBF; Figures 1 and S2) is involved in membrane structuring.

The role of *Tb*MfnL in mitochondrial shaping was observed by its overexpression in PCF trypanosomes, which induced a very strong increase in number of connections in the single branched mitochondrion. Moreover, the inactivation of its GTPase domain

(G) Schematic representation of truncated transmembrane domains of *Tb*MfnL protein (45 amino acids) tagged with 3Ty1 peptide at the C terminus of the protein ($^{oe}$*Tb*MfnL-ΔTM$_{::3Ty1}$). See also Figures S1, S4, S8, and S9.
(H) Western blotting of whole-cell extracts of *T. brucei* PCF overexpressing *Tb*MfnL-ΔTM$_{::3Ty1}$ cells; (−Tet) non-induced and (+Tet) induced cells for 3 days.
(I) Subcellular localization of $^{oe}$*Tb*MfnL-ΔTM$_{::3Ty1}$ in PCF after 3 days of induction, analyzed by standard immunofluorescence. n, nucleus; k, kinetoplast. The scale bar represents 5 μm. See also Figures S1, S4, S8, and S9.

Please cite this article in press as: Morel et al., A new member of the dynamin superfamily modulates mitochondrial membrane branching in *Trypanosoma brucei*, Current Biology (2025), https://doi.org/10.1016/j.cub.2025.02.033



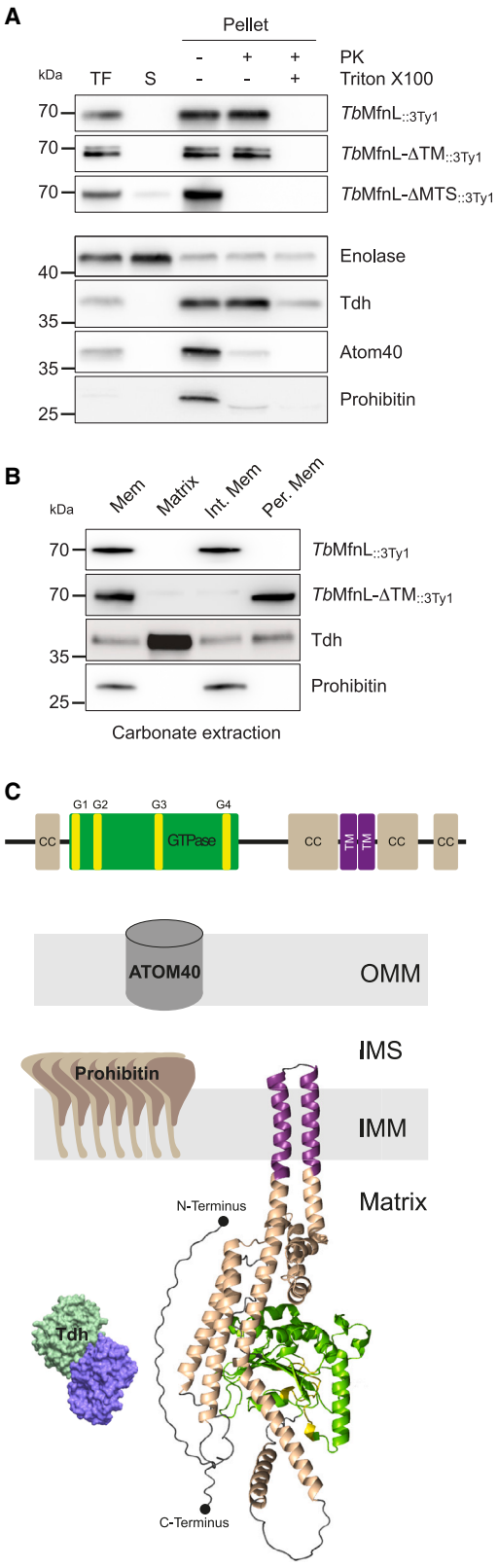


**Figure 7. Membrane topology of *Tb*MfnL**

(A) The Proteinase K protection assay involved incubating mitoplasts with Proteinase K and Triton X-100, as denoted by the "+" symbol. TF represents the total fraction containing both cytoplasmic and membrane components; S denotes the supernatant, comprising the cytosolic contents; and pellet represents the organelle fraction.

(B) Carbonate extraction of mitochondria isolated from $^{oe}$*Tb*MfnL$_{::3Ty1}$ and $^{oe}$*Tb*MfnL-ΔTM$_{::3Ty1}$ cells. Mem, membrane fraction; Matrix, matrix fraction; Int. Mem, integral membrane fraction; Per. Mem, peripheral membrane fraction.

(C) Predicted structure of *Tb*MfnL, from AlphaFold protein structure database. *Tb*MfnL was embedded in the mitochondrial inner membrane. The color coding corresponds to the predicted secondary structure depicted on the top of the figure. The first 41 N-terminal amino acids corresponding to the MTS are not shown as they are cleaved. The N and C termini are marked by small black spheres. The AlphaFold model score of *Tb*MfnL is between confident to very high for most of the structured domains (https://alphafold.ebi.ac.uk/entry/Q57XN3). OMM, outer mitochondrial membrane; IMS, inter-mitochondrial space; IMM, inner mitochondrial membrane.

via mutation of the G1 motif also confirms its belonging to the large family of dynamins. Interestingly, a link between hyperconnection of a branching network and increased fusion processes has been reported in a highly different biological system, filamentous fungi, which grow as interconnected branching networks.[66] This raises the intriguing possibility that an excess of *Tb*MfnL in PCF trypanosomes enhances the interconnectivity of mitochondrial networks by inducing mitochondrial fusion.

The absence of fragmentation observed upon partial or total inactivation of *Tb*MfnL expression is in agreement with the absence or a very low level of constitutive mitochondrial fission. By contrast, in mammals and yeast, inhibition of fusion results in mitochondrial fragmentation by constitutive fission.[16,67] Thus, our results are in agreement with previous studies suggesting that fission only occurs during cell division.[19,28] The lack of observable mitochondrial alterations may also be attributed to the involvement of other proteins in mitochondrial structuring, as suggested by studies on the mitochondrial outer membrane proteome in *T. brucei*[68,69] and the presence of mitochondrial complexes such as the recently characterized MICOS.[47] Additionally, subtle changes in mitochondrial structure may exist but could have gone undetected using our current approaches. It is worth noting that *Tb*MfnL seems to participate in a unique membrane-structuring mechanism, and its inactivation may not produce effects similar to those observed for Mfn or Opa1.

Another intriguing point was the discrepancy with the results reported by Vanwalleghem et al.[30] Indeed, they describe fenestration of the mitochondrion in BSF cells with downregulated *Tb*MfnL, whereas in our studies, involving inactivation by CRISPR-Cas9 or downregulation by RNAi in BSF cells, we did not observe any alterations in mitochondrial structure. The only modification (hyper-reticulation) of the mitochondrial structure was observed exclusively during the overexpression of *Tb*MfnL and only in PCFs. This discrepancy may arise from differences in cell lines, culturing conditions, sample preparation methods, or mitochondrial staining protocols. We used rhodamine staining on live cells and immunofluorescence labeling to visualize the mitochondrial network, whereas Vanwalleghem et al.[30] employed FIB-SEM tomography. It is also possible that *Tb*MfnL knockdown affects mitochondrial import, since disruptions in mitochondrial import have been reported to influence mitochondrial structure.[68]

Using several microscopy approaches, we have demonstrated that *Tb*MfnL is localized within the mitochondrial membranes, with two domains involved in its accurate mitochondrial addressing, a canonical N-terminal MTS and two adjacent C-terminal transmembrane domains. Expression of MTS-less *Tb*MfnL or MTS-GFP recombinant proteins in PCF trypanosomes confirmed the role of this 41 aa-long MTS for mitochondrial import. Proteins with an N-terminal MTS are typically imported into the mitochondrial matrix, with a few exceptions, such as Opa1 and apoptosis-inducing factor (AIF), facing the intermembrane space.[70] Indeed, Opa1 and AIF localize mainly to the intermitochondrial space due to their TMs located in close proximity to the MTS (Figure 1A), interrupting transport across the inner membrane. The C-proximal localization of the transmembrane domains of *Tb*MfnL is not compatible with such import interruption but more presumably suggested that its C terminus is also exposed to the matrix, as predicted by AlphaFold (Figure 7C). This model is consistent with the Proteinase K resistance of *Tb*MfnL in mitoplasts. This orientation is also probably similar to that of the prokaryotic MfnLs identified in this study, which could also be anchored in the plasma membrane and oriented toward the cytosol. Interestingly, recent publications describe mitochondrial remodeling originating from the matrix side of the mitochondria. Sheikh et al.[71] demonstrated that expressing a potential DSP from a giant virus in *T. brucei* PCF significantly affects mitochondrial morphology within the matrix, with a notable association with the inner membrane. Additionally, Kumar et al.[72] and Mears[73] showed that a dynamin superfamily-like pseudoenzyme, a distant relative of the dynamin superfamily, stabilizes cristae architecture through interactions on the matrix side of the mitochondrial inner membrane. This contrasts with the mode of action of human or yeast Mfns, which are involved in the remodeling of mitochondrial outer and inner membranes, but never via the matrix side.

In conclusion, the data presented here uncover a new family of DSPs and suggest the existence of a novel membrane-structuring mechanism found in both eukaryotes and prokaryotes but distinct from those involved in mitochondrial membrane fusion in mammals and fungi.

## RESOURCE AVAILABILITY

### Lead contact

Requests for further information and resources should be directed to and will be fulfilled by the lead contact, Emmanuel Tetaud (emmanuel.tetaud@u-bordeaux.fr).

### Materials availability

All unique reagents generated in this study are available from the lead contact without restriction.

### Data and code availability

- The data illustrating the mitochondrial morphology of parental wild-type, $^{oe}$*Tb*MfnL$_{::3Ty1}$, and $^{oe}$*Tb*MfnL-K141A$_{::3Ty1}$ PCF cells; the complete western blot data from the membrane topology study; and the AlphaFold-predicted structure of *Tb*MfnL and the pLDDT scores for each amino acid have been uploaded to the Mendeley online repository and are publicly accessible at https://doi.org/10.17632/jr3jbf6fp8.1 as of the publication date.
- All original code is available in this paper's supplemental information.
- Any additional information required to reanalyze the data reported in this paper is available from the lead contact upon request.

## ACKNOWLEDGMENTS

We thank Julius Lukeš (Biology Centre, Czech Academy of Sciences) for providing us with the anti-Prohibitin antibody; André Schneider (University of Bern) for providing us with the anti-Atom40 antibody; Keith Gull (University of Manchester) for providing us with the anti-Ty1 antibody; and Derrick Robinson, Mélanie Bonhivers, Elina Casas, and Nicolas Landrein (University of Bordeaux) for the pPOTv7 expression vector and extremely valuable help in the expansion microscopy experiment. Cell sorter analyses were performed at the TBMCore facility (FACSility) on BD FACSAria III Sorter, and we thank Atika Zouine for data acquisition and interpretation. We also thank Bordeaux Imaging Center (BIC), which is a member of the FranceBioImaging national infrastructure (ANR10-INBS-04), for helping us to design the ImageJ macro and microscopy acquisitions. The Bringaud team is supported by the Centre National de la Recherche Scientifique (CNRS, https://www.cnrs.fr/), the Université de Bordeaux (https://www.u-bordeaux.fr/), and the Agence Nationale de la Recherche (ANR, https://anr.fr/) through the ParaFrap "Laboratoire d'Excellence" (LabEx, https://www.enseignementsup-recherche.gouv.fr/cid51355/laboratoires-d-excellence.html) (ANR-11-LABX-0024). This work was supported by the "Fondation pour la Recherche Médicale" (FRM, https://www.frm.org/) ("Equipe FRM," grant no. EQU201903007845), ANR grant ADIPOTRYP (ANR19-CE15-0004-01) to F.B., and ERC advanced grant 787904 to D.M. Portions of this manuscript were based on C.A.M.'s thesis defended at the University of Bordeaux.

## AUTHOR CONTRIBUTIONS

C.A.M. conceptualized the study, performed experiments, and contributed to analysis and writing. C.A. performed experiments and contributed to analysis. D.M. performed all the phylogenetic analysis. C.B., B.S., and E.G. performed the EM and SBF-SEM experiments and contributed to their analysis. D.M., S.D.-C., M.R., F.B., and E.T. conceptualized the study, contributed to analysis, and wrote the manuscript with input from all the authors.

## DECLARATION OF INTERESTS

The authors declare no competing interests.

## STAR★METHODS

Detailed methods are provided in the online version of this paper and include the following:



## SUPPLEMENTAL INFORMATION

Supplemental information can be found online at https://doi.org/10.1016/j.cub.2025.02.033.

Received: July 25, 2024
Revised: December 23, 2024
Accepted: February 17, 2025
Published: March 12, 2025

## REFERENCES

1. Böhringer, S., and Hecker, H. (1975). Quantitative ultrastructural investigations of the life cycle of Trypanosoma brucei: a morphometric analysis. J. Protozool. *22*, 463–467. https://doi.org/10.1111/j.1550-7408.1975.tb05210.x.
2. Bílý, T., Sheikh, S., Mallet, A., Bastin, P., Pérez-Morga, D., Lukeš, J., and Hashimi, H. (2021). Ultrastructural changes of the mitochondrion during the life cycle of Trypanosoma brucei. J. Eukaryot. Microbiol. *68*, e12846. https://doi.org/10.1111/jeu.12846.
3. Priest, J.W., and Hajduk, S.L. (1994). Developmental regulation of Trypanosoma brucei cytochrome c reductase during bloodstream to procyclic differentiation. Mol. Biochem. Parasitol. *65*, 291–304. https://doi.org/10.1016/0166-6851(94)90080-9.
4. van Hellemond, J.J., Opperdoes, F.R., and Tielens, A.G. (2005). The extraordinary mitochondrion and unusual citric acid cycle in Trypanosoma brucei. Biochem. Soc. Trans. *33*, 967–971. https://doi.org/10.1042/BST20050967.
5. Michels, P.A.M., Bringaud, F., Herman, M., and Hannaert, V. (2006). Metabolic functions of glycosomes in trypanosomatids. Biochim. Biophys. Acta *1763*, 1463–1477. https://doi.org/10.1016/j.bbamcr.2006.08.019.
6. Bringaud, F., Rivière, L., and Coustou, V. (2006). Energy metabolism of trypanosomatids: adaptation to available carbon sources. Mol. Biochem. Parasitol. *149*, 1–9. https://doi.org/10.1016/j.molbiopara.2006.03.017.
7. Duvezin-Caubet, S., Jagasia, R., Wagener, J., Hofmann, S., Trifunovic, A., Hansson, A., Chomyn, A., Bauer, M.F., Attardi, G., Larsson, N.G., et al. (2006). Proteolytic processing of OPA1 links mitochondrial dysfunction to alterations in mitochondrial morphology. J. Biol. Chem. *281*, 37972–37979. https://doi.org/10.1074/jbc.M606059200.
8. Sauvanet, C., Duvezin-Caubet, S., di Rago, J.P., and Rojo, M. (2010). Energetic requirements and bioenergetic modulation of mitochondrial morphology and dynamics. Semin. Cell Dev. Biol. *21*, 558–565. https://doi.org/10.1016/j.semcdb.2009.12.006.
9. Silva Ramos, E., Larsson, N.G., and Mourier, A. (2016). Bioenergetic roles of mitochondrial fusion. Biochim. Biophys. Acta *1857*, 1277–1283. https://doi.org/10.1016/j.bbabio.2016.04.002.
10. Chan, D.C. (2012). Fusion and fission: interlinked processes critical for mitochondrial health. Annu. Rev. Genet. *46*, 265–287. https://doi.org/10.1146/annurev-genet-110410-132529.
11. Westermann, B. (2010). Mitochondrial fusion and fission in cell life and death. Nat. Rev. Mol. Cell Biol. *11*, 872–884. https://doi.org/10.1038/nrm3013.
12. Sesaki, H., Adachi, Y., Kageyama, Y., Itoh, K., and Iijima, M. (2014). In vivo functions of Drp1: lessons learned from yeast genetics and mouse knockouts. Biochim. Biophys. Acta *1842*, 1179–1185. https://doi.org/10.1016/j.bbadis.2013.11.024.
13. Otera, H., Ishihara, N., and Mihara, K. (2013). New insights into the function and regulation of mitochondrial fission. Biochim. Biophys. Acta *1833*, 1256–1268. https://doi.org/10.1016/j.bbamcr.2013.02.002.
14. Malka, F., Guillery, O., Cifuentes-Diaz, C., Guillou, E., Belenguer, P., Lombès, A., and Rojo, M. (2005). Separate fusion of outer and inner mitochondrial membranes. EMBO Rep. *6*, 853–859. https://doi.org/10.1038/sj.embor.7400488.
15. Song, Z., Ghochani, M., McCaffery, J.M., Frey, T.G., and Chan, D.C. (2009). Mitofusins and OPA1 mediate sequential steps in mitochondrial membrane fusion. Mol. Biol. Cell *20*, 3525–3532. https://doi.org/10.1091/mbc.E09-03-0252.
16. Legros, F., Lombès, A., Frachon, P., and Rojo, M. (2002). Mitochondrial fusion in human cells is efficient, requires the inner membrane potential, and is mediated by mitofusins. Mol. Biol. Cell *13*, 4343–4354. https://doi.org/10.1091/mbc.E02-06-0330.
17. Bertholet, A.M., Delerue, T., Millet, A.M., Moulis, M.F., David, C., Daloyau, M., Arnauné-Pelloquin, L., Davezac, N., Mils, V., Miquel, M.C., et al. (2016). Mitochondrial fusion/fission dynamics in neurodegeneration and neuronal plasticity. Neurobiol. Dis. *90*, 3–19. https://doi.org/10.1016/j.nbd.2015.10.011.
18. Hughes, L., Borrett, S., Towers, K., Starborg, T., and Vaughan, S. (2017). Patterns of organelle ontogeny through a cell cycle revealed by whole-cell reconstructions using 3D electron microscopy. J. Cell Sci. *130*, 637–647. https://doi.org/10.1242/jcs.198887.
19. Chanez, A.L., Hehl, A.B., Engstler, M., and Schneider, A. (2006). Ablation of the single dynamin of T. brucei blocks mitochondrial fission and endocytosis and leads to a precise cytokinesis arrest. J. Cell Sci. *119*, 2968–2974. https://doi.org/10.1242/jcs.03023.
20. Jakob, M., Hoffmann, A., Amodeo, S., Peitsch, C., Zuber, B., and Ochsenreiter, T. (2016). Mitochondrial growth during the cell cycle of Trypanosoma brucei bloodstream forms. Sci. Rep. *6*, 36565. https://doi.org/10.1038/srep36565.
21. Esseiva, A.C., Chanez, A.L., Bochud-Allemann, N., Martinou, J.C., Hemphill, A., and Schneider, A. (2004). Temporal dissection of Bax-induced events leading to fission of the single mitochondrion in Trypanosoma brucei. EMBO Rep. *5*, 268–273. https://doi.org/10.1038/sj.embor.7400095.
22. Gibson, W., Crow, M., and Kearns, J. (1997). Kinetoplast DNA minicircles are inherited from both parents in genetic crosses of Trypanosoma brucei. Parasitol. Res. *83*, 483–488. https://doi.org/10.1007/s004360050284.
23. DiMaio, J., Ruthel, G., Cannon, J.J., Malfara, M.F., and Povelones, M.L. (2018). The single mitochondrion of the kinetoplastid parasite Crithidia fasciculata is a dynamic network. PLoS One *13*, e0202711. https://doi.org/10.1371/journal.pone.0202711.
24. van der Bliek, A.M., Shen, Q., and Kawajiri, S. (2013). Mechanisms of mitochondrial fission and fusion. Cold Spring Harb. Perspect. Biol. *5*, a011072. https://doi.org/10.1101/cshperspect.a011072.
25. Logan, D.C. (2006). Plant mitochondrial dynamics. Biochim. Biophys. Acta *1763*, 430–441. https://doi.org/10.1016/j.bbamcr.2006.01.003.
26. Arimura, S.I. (2018). Fission and fusion of plant mitochondria, and genome maintenance. Plant Physiol. *176*, 152–161. https://doi.org/10.1104/pp.17.01025.
27. Gao, H., Sage, T.L., and Osteryoung, K.W. (2006). FZL, an FZO-like protein in plants, is a determinant of thylakoid and chloroplast morphology. Proc. Natl. Acad. Sci. USA *103*, 6759–6764. https://doi.org/10.1073/pnas.0507287103.
28. Morgan, G.W., Goulding, D., and Field, M.C. (2004). The single dynamin-like protein of Trypanosoma brucei regulates mitochondrial division and is not required for endocytosis. J. Biol. Chem. *279*, 10692–10701. https://doi.org/10.1074/jbc.M312178200.
29. Benz, C., Stříbrná, E., Hashimi, H., and Lukeš, J. (2017). Dynamin-like proteins in Trypanosoma brucei: A division of labour between two paralogs? PLoS One *12*, e0177200. https://doi.org/10.1371/journal.pone.0177200.
30. Vanwalleghem, G., Fontaine, F., Lecordier, L., Tebabi, P., Klewe, K., Nolan, D.P., Yamaryo-Botté, Y., Botté, C., Kremer, A., Burkard, G.S., et al. (2015). Coupling of lysosomal and mitochondrial membrane permeabilization in trypanolysis by APOL1. Nat. Commun. *6*, 8078. https://doi.org/10.1038/ncomms9078.
31. Mattie, S., Riemer, J., Wideman, J.G., and McBride, H.M. (2018). A new mitofusin topology places the redox-regulated C terminus in the mitochondrial intermembrane space. J. Cell Biol. *217*, 507–515. https://doi.org/10.1083/jcb.201611194.
32. Jones, D.T. (1999). Protein secondary structure prediction based on position-specific scoring matrices. J. Mol. Biol. *292*, 195–202. https://doi.org/10.1006/jmbi.1999.3091.

33. Urbaniak, M.D., Guther, M.L.S., and Ferguson, M.A.J. (2012). Comparative SILAC proteomic analysis of Trypanosoma brucei bloodstream and procyclic lifecycle stages. PLoS ONE *7*, e36619. https://doi.org/10.1371/journal.pone.0036619.

34. Siegel, T.N., Hekstra, D.R., Wang, X., Dewell, S., and Cross, G.A.M. (2010). Genome-wide analysis of mRNA abundance in two life-cycle stages of Trypanosoma brucei and identification of splicing and polyadenylation sites. Nucleic Acids Res. *38*, 4946–4957. https://doi.org/10.1093/nar/gkq237.

35. Millerioux, Y., Ebikeme, C., Biran, M., Morand, P., Bouyssou, G., Vincent, I.M., Mazet, M., Riviere, L., Franconi, J.M., Burchmore, R.J.S., et al. (2013). The threonine degradation pathway of the Trypanosoma brucei procyclic form: the main carbon source for lipid biosynthesis is under metabolic control. Mol. Microbiol. *90*, 114–129. https://doi.org/10.1111/mmi.12351.

36. Billington, K., Halliday, C., Madden, R., Dyer, P., Barker, A.R., Moreira-Leite, F.F., Carrington, M., Vaughan, S., Hertz-Fowler, C., Dean, S., et al. (2023). Genome-wide subcellular protein map for the flagellate parasite Trypanosoma brucei. Nat. Microbiol. *8*, 533–547. https://doi.org/10.1038/s41564-022-01295-6.

37. Hannaert, V., Albert, M.A., Rigden, D.J., da Silva Giotto, M.T., Thiemann, O., Garratt, R.C., Van Roy, J., Opperdoes, F.R., and Michels, P.A.M. (2003). Kinetic characterization, structure modelling studies and crystallization of Trypanosoma brucei enolase. Eur. J. Biochem. *270*, 3205–3213. https://doi.org/10.1046/j.1432-1033.2003.03692.x.

38. Nunnari, J., Marshall, W.F., Straight, A., Murray, A., Sedat, J.W., and Walter, P. (1997). Mitochondrial transmission during mating in Saccharomyces cerevisiae is determined by mitochondrial fusion and fission and the intramitochondrial segregation of mitochondrial DNA. Mol. Biol. Cell *8*, 1233–1242. https://doi.org/10.1091/mbc.8.7.1233.

39. Asencio, C., Hervé, P., Morand, P., Oliveres, Q., Morel, C.A., Prouzet-Mauleon, V., Biran, M., Monic, S., Bonhivers, M., Robinson, D.R., et al. (2024). Streptococcus pyogenes Cas9 ribonucleoprotein delivery for efficient, rapid and marker-free gene editing in Trypanosoma and Leishmania. Mol. Microbiol. *121*, 1079–1094. https://doi.org/10.1111/mmi.15256.

40. Hales, K.G., and Fuller, M.T. (1997). Developmentally regulated mitochondrial fusion mediated by a conserved, novel, predicted GTPase. Cell *90*, 121–129. https://doi.org/10.1016/s0092-8674(00)80319-0.

41. Hermann, G.J., Thatcher, J.W., Mills, J.P., Hales, K.G., Fuller, M.T., Nunnari, J., and Shaw, J.M. (1998). Mitochondrial fusion in yeast requires the transmembrane GTPase Fzo1p. J. Cell Biol. *143*, 359–373. https://doi.org/10.1083/jcb.143.2.359.

42. Santel, A., Frank, S., Gaume, B., Herrler, M., Youle, R.J., and Fuller, M.T. (2003). Mitofusin-1 protein is a generally expressed mediator of mitochondrial fusion in mammalian cells. J. Cell Sci. *116*, 2763–2774. https://doi.org/10.1242/jcs.00479.

43. Gambarotto, D., Hamel, V., and Guichard, P. (2021). Ultrastructure expansion microscopy (U-ExM). Methods Cell Biol. *161*, 57–81. https://doi.org/10.1016/bs.mcb.2020.05.006.

44. Amodeo, S., Kalichava, A., Fradera-Sola, A., Bertiaux-Lequoy, E., Guichard, P., Butter, F., and Ochsenreiter, T. (2021). Characterization of the novel mitochondrial genome segregation factor TAP110 in Trypanosoma brucei. J. Cell Sci. *134*, jcs254300. https://doi.org/10.1242/jcs.254300.

45. Gorilak, P., Pružincová, M., Vachova, H., Olšinová, M., Schmidt Cernohorska, M., and Varga, V. (2021). Expansion microscopy facilitates quantitative super-resolution studies of cytoskeletal structures in kinetoplastid parasites. Open Biol. *11*, 210131. https://doi.org/10.1098/rsob.210131.

46. Rojo, M., Legros, F., Chateau, D., and Lombès, A. (2002). Membrane topology and mitochondrial targeting of mitofusins, ubiquitous mammalian homologs of the transmembrane GTPase Fzo. J. Cell Sci. *115*, 1663–1674. https://doi.org/10.1242/jcs.115.8.1663.

47. Kaurov, I., Vancová, M., Schimanski, B., Cadena, L.R., Heller, J., Bílý, T., Potěšil, D., Eichenberger, C., Bruce, H., Oeljeklaus, S., et al. (2018). The diverged trypanosome MICOS complex as a hub for mitochondrial cristae shaping and protein import. Curr. Biol. *28*, 3393–3407.e5. https://doi.org/10.1016/j.cub.2018.09.008.

48. Wenger, C., Oeljeklaus, S., Warscheid, B., Schneider, A., and Harsman, A. (2017). A trypanosomal orthologue of an intermembrane space chaperone has a non-canonical function in biogenesis of the single mitochondrial inner membrane protein translocase. PLoS Pathog. *13*, e1006550. https://doi.org/10.1371/journal.ppat.1006550.

49. Pyrih, J., Hammond, M., Alves, A., Dean, S., Sunter, J.D., Wheeler, R.J., Gull, K., and Lukeš, J. (2023). Comprehensive sub-mitochondrial protein map of the parasitic protist Trypanosoma brucei defines critical features of organellar biology. Cell Rep. *42*, 113083. https://doi.org/10.1016/j.celrep.2023.113083.

50. Daumke, O., and Praefcke, G.J.K. (2016). Invited review: mechanisms of GTP hydrolysis and conformational transitions in the dynamin superfamily. Biopolymers *105*, 580–593. https://doi.org/10.1002/bip.22855.

51. Ramachandran, R., and Schmid, S.L. (2018). The dynamin superfamily. Curr. Biol. *28*, R411–R416. https://doi.org/10.1016/j.cub.2017.12.013.

52. Shepard, K.A., and Yaffe, M.P. (1999). The yeast dynamin-like protein, Mgm1p, functions on the mitochondrial outer membrane to mediate mitochondrial inheritance. J. Cell Biol. *144*, 711–720. https://doi.org/10.1083/jcb.144.4.711.

53. Derelle, R., Torruella, G., Klimeš, V., Brinkmann, H., Kim, E., Vlček, Č., Lang, B.F., and Eliáš, M. (2015). Bacterial proteins pinpoint a single eukaryotic root. Proc. Natl. Acad. Sci. USA *112*, E693–E699. https://doi.org/10.1073/pnas.1420657112.

54. Sawant, P., Eissenberger, K., Karier, L., Mascher, T., and Bramkamp, M. (2016). A dynamin-like protein involved in bacterial cell membrane surveillance under environmental stress. Environ. Microbiol. *18*, 2705–2720. https://doi.org/10.1111/1462-2920.13110.

55. de Sousa Borges, A., and Scheffers, D.J. (2016). Bacterial dynamin as a membrane puncture repair kit. Environ. Microbiol. *18*, 2298–2301. https://doi.org/10.1111/1462-2920.13218.

56. Michie, K.A., Boysen, A., Low, H.H., Møller-Jensen, J., and Löwe, J. (2014). LeoA, B and C from enterotoxigenic Escherichia coli (ETEC) are bacterial dynamins. PLoS One *9*, e107211. https://doi.org/10.1371/journal.pone.0107211.

57. Schlimpert, S., Wasserstrom, S., Chandra, G., Bibb, M.J., Findlay, K.C., Flärdh, K., and Buttner, M.J. (2017). Two dynamin-like proteins stabilize FtsZ rings during Streptomyces sporulation. Proc. Natl. Acad. Sci. USA *114*, E6176–E6183. https://doi.org/10.1073/pnas.1704612114.

58. Bramkamp, M. (2012). Structure and function of bacterial dynamin-like proteins. Biol. Chem. *393*, 1203–1214. https://doi.org/10.1515/hsz-2012-0185.

59. Bürmann, F., Ebert, N., van Baarle, S., and Bramkamp, M. (2011). A bacterial dynamin-like protein mediating nucleotide-independent membrane fusion. Mol. Microbiol. *79*, 1294–1304. https://doi.org/10.1111/j.1365-2958.2011.07523.x.

60. Jimah, J.R., and Hinshaw, J.E. (2019). Structural insights into the mechanism of dynamin superfamily proteins. Trends Cell Biol. *29*, 257–273. https://doi.org/10.1016/j.tcb.2018.11.003.

61. Liu, J., Noel, J.K., and Low, H.H. (2018). Structural basis for membrane tethering by a bacterial dynamin-like pair. Nat. Commun. *9*, 3345. https://doi.org/10.1038/s41467-018-05523-8.

62. Lindsay, M.R., Webb, R.I., and Fuerst, J.A. (1997). Pirellulosomes: a new type of membrane-bounded cell compartment in planctomycete bacteria of the genus Pirellula. Microbiology (Reading) *143*, 739–748. https://doi.org/10.1099/00221287-143-3-739.

63. Fuerst, J.A., and Webb, R.I. (1991). Membrane-bounded nucleoid in the eubacterium Gemmata obscuriglobus. Proc. Natl. Acad. Sci. USA *88*, 8184–8188. https://doi.org/10.1073/pnas.88.18.8184.

64. Jogler, C. (2014). The bacterial 'mitochondrium'. Mol. Microbiol. *94*, 751–755. https://doi.org/10.1111/mmi.12814.

65. Neumann, S., Wessels, H.J.C.T., Rijpstra, W.I.C., Sinninghe Damsté, J.S., Kartal, B., Jetten, M.S.M., and van Niftrik, L. (2014). Isolation and characterization of a prokaryotic cell organelle from the anammox bacterium

Kuenenia stuttgartiensis. Mol. Microbiol. *94*, 794–802. https://doi.org/10.1111/mmi.12816.

66. Herzog, S., Schumann, M.R., and Fleißner, A. (2015). Cell fusion in Neurospora crassa. Curr. Opin. Microbiol. *28*, 53–59. https://doi.org/10.1016/j.mib.2015.08.002.
67. Sesaki, H., and Jensen, R.E. (1999). Division versus fusion: Dnm1p and Fzo1p antagonistically regulate mitochondrial shape. J. Cell Biol. *147*, 699–706. https://doi.org/10.1083/jcb.147.4.699.
68. Niemann, M., Wiese, S., Mani, J., Chanfon, A., Jackson, C., Meisinger, C., Warscheid, B., and Schneider, A. (2013). Mitochondrial outer membrane proteome of Trypanosoma brucei reveals novel factors required to maintain mitochondrial morphology. Mol. Cell. Proteomics *12*, 515–528. https://doi.org/10.1074/mcp.M112.023093.
69. Povelones, M.L., Tiengwe, C., Gluenz, E., Gull, K., Englund, P.T., and Jensen, R.E. (2013). Mitochondrial shape and function in trypanosomes requires the outer membrane protein, TbLOK1. Mol. Microbiol. *87*, 713–729. https://doi.org/10.1111/mmi.12089.
70. Otera, H., Ohsakaya, S., Nagaura, Z.I., Ishihara, N., and Mihara, K. (2005). Export of mitochondrial AIF in response to proapoptotic stimuli depends on processing at the intermembrane space. EMBO J. *24*, 1375–1386. https://doi.org/10.1038/sj.emboj.7600614.
71. Sheikh, S., Pánek, T., Gahura, O., Týč, J., Záhonová, K., Lukeš, J., Eliáš, M., and Hashimi, H. (2023). A novel group of dynamin-related proteins shared by eukaryotes and giant viruses is able to remodel mitochondria from within the matrix. Mol. Biol. Evol. *40*, msad134. https://doi.org/10.1093/molbev/msad134.
72. Kumar, A., Gok, M.O., Nguyen, K.N., Connor, O.M., Reese, M.L., Wideman, J.G., Muñoz-Gómez, S.A., and Friedman, J.R. (2024). A dynamin superfamily-like pseudoenzyme coordinates with MICOS to promote cristae architecture. Curr. Biol. *34*, 2606–2622.e9. https://doi.org/10.1016/j.cub.2024.04.028.
73. Mears, J.A. (2024). Mitochondrial biology: unique membrane remodeling from the matrix. Curr. Biol. *34*, R581–R583. https://doi.org/10.1016/j.cub.2024.05.010.
74. Bastin, P., Bagherzadeh, Z., Matthews, K.R., and Gull, K. (1996). A novel epitope tag system to study protein targeting and organelle biogenesis in Trypanosoma brucei. Mol. Biochem. Parasitol. *77*, 235–239. https://doi.org/10.1016/0166-6851(96)02598-4.
75. Týc, J., Faktorová, D., Kriegová, E., Jirků, M., Vávrová, Z., Maslov, D.A., and Lukes, J. (2010). Probing for primary functions of prohibitin in Trypanosoma brucei. Int. J. Parasitol. *40*, 73–83. https://doi.org/10.1016/j.ijpara.2009.07.008.
76. Mani, J., Desy, S., Niemann, M., Chanfon, A., Oeljeklaus, S., Pusnik, M., Schmidt, O., Gerbeth, C., Meisinger, C., Warscheid, B., et al. (2015). Mitochondrial protein import receptors in kinetoplastids reveal convergent evolution over large phylogenetic distances. Nat. Commun. *6*, 6646. https://doi.org/10.1038/ncomms7646.
77. Besteiro, S., Biran, M., Biteau, N., Coustou, V., Baltz, T., Canioni, P., and Bringaud, F. (2002). Succinate secreted by Trypanosoma brucei is produced by a novel and unique glycosomal enzyme, NADH-dependent fumarate reductase. J. Biol. Chem. *277*, 38001–38012. https://doi.org/10.1074/jbc.M201759200.
78. Bringaud, F., Peyruchaud, S., Baltz, D., Giroud, C., Simpson, L., and Baltz, T. (1995). Molecular characterization of the mitochondrial heat shock protein 60 gene from Trypanosoma brucei. Mol. Biochem. Parasitol. *74*, 119–123. https://doi.org/10.1016/0166-6851(95)02486-7.
79. Bringaud, F., Baltz, D., and Baltz, T. (1998). Functional and molecular characterization of a glycosomal PPI-dependent enzyme in trypanosomatids: pyruvate, phosphate dikinase. Proc. Natl. Acad. Sci. USA *95*, 7963–7968. https://doi.org/10.1073/pnas.95.14.7963.
80. Wirtz, E., Leal, S., Ochatt, C., and Cross, G.A. (1999). A tightly regulated inducible expression system for conditional gene knock-outs and dominant-negative genetics in Trypanosoma brucei. Mol. Biochem. Parasitol. *99*, 89–101. https://doi.org/10.1016/s0166-6851(99)00002-x.
81. Paterou, A., Týč, J., Sunter, J., Vaughan, S., Gull, K., and Dean, S. (2023). Unlocking trypanosome biology: A comprehensive protein-tagging toolkit for localization and functional analysis. Preprint at bioRxiv. https://doi.org/10.1101/2023.04.21.537815.
82. Wickstead, B., Ersfeld, K., and Gull, K. (2002). Targeting of a tetracycline-inducible expression system to the transcriptionally silent minichromosomes of Trypanosoma brucei. Mol. Biochem. Parasitol. *125*, 211–216. https://doi.org/10.1016/s0166-6851(02)00238-4.
83. Biebinger, S., Wirtz, L.E., Lorenz, P., and Clayton, C. (1997). Vectors for inducible expression of toxic gene products in bloodstream and procyclic Trypanosoma brucei. Mol. Biochem. Parasitol. *85*, 99–112. https://doi.org/10.1016/s0166-6851(96)02815-0.
84. Schindelin, J., Arganda-Carreras, I., Frise, E., Kaynig, V., Longair, M., Pietzsch, T., Preibisch, S., Rueden, C., Saalfeld, S., Schmid, B., et al. (2012). Fiji: an open-source platform for biological-image analysis. Nat. Methods *9*, 676–682. https://doi.org/10.1038/nmeth.2019.
85. Hirumi, H., and Hirumi, K. (1989). Continuous cultivation of Trypanosoma brucei blood stream forms in a medium containing a low concentration of serum protein without feeder cell layers. J. Parasitol. *75*, 985–989. https://doi.org/10.2307/3282883.
86. Altschul, S.F., Gish, W., Miller, W., Myers, E.W., and Lipman, D.J. (1990). Basic local alignment search tool. J. Mol. Biol. *215*, 403–410. https://doi.org/10.1016/S0022-2836(05)80360-2.
87. Richter, D.J., Berney, C., Strassert, J.F.H., Poh, Y.-P., Herman, E.K., Muñoz-Gómez, S.A., Wideman, J.G., Burki, F., and de Vargas, C. (2022). EukProt: A database of genome-scale predicted proteins across the diversity of eukaryotes. Preprint at bioRxiv. https://doi.org/10.1101/2020.06.30.180687.
88. Katoh, K., and Standley, D.M. (2013). MAFFT multiple sequence alignment software version 7: improvements in performance and usability. Mol. Biol. Evol. *30*, 772–780. https://doi.org/10.1093/molbev/mst010.
89. Criscuolo, A., and Gribaldo, S. (2010). BMGE (Block Mapping and Gathering with Entropy): a new software for selection of phylogenetic informative regions from multiple sequence alignments. BMC Evol. Biol. *10*, 210. https://doi.org/10.1186/1471-2148-10-210.
90. Minh, B.Q., Schmidt, H.A., Chernomor, O., Schrempf, D., Woodhams, M.D., von Haeseler, A., and Lanfear, R. (2020). IQ-TREE 2: New models and efficient methods for phylogenetic inference in the genomic era. Mol. Biol. Evol. *37*, 1530–1534. https://doi.org/10.1093/molbev/msaa015.
91. Claros, M.G., and Vincens, P. (1996). Computational method to predict mitochondrially imported proteins and their targeting sequences. Eur. J. Biochem. *241*, 779–786. https://doi.org/10.1111/j.1432-1033.1996.00779.x.
92. Casas, E., Landrein, N., and Bonhivers, M. (2012). Ultra expansion microscopy protocol with improved setup for upright and inverted microscopes. protocols.io. https://doi.org/10.17504/protocols.io.bvwqn7dw.
93. Dean, S., Sunter, J., Wheeler, R.J., Hodkinson, I., Gluenz, E., and Gull, K. (2015). A toolkit enabling efficient, scalable and reproducible gene tagging in trypanosomatids. Open Biol. *5*, 140197. https://doi.org/10.1098/rsob.140197.
94. Ling, M.M., and Robinson, B.H. (1997). Approaches to DNA mutagenesis: an overview. Anal. Biochem. *254*, 157–178. https://doi.org/10.1006/abio.1997.2428.
95. Blancard, C., Decoeur, F., Duvezin-Caubet, S., Giraud, M.F., and Salin, B. (2024). Advancing yeast cell analysis: A cryomethod for serial block-face scanning electron microscopy imaging in mitochondrial morphology studies. Biol. Cell *117*, e202400038. https://doi.org/10.1111/boc.202400038.
96. Blancard, C., and Salin, B. (2017). Plunge freezing: A tool for the ultrastructural and immunolocalization studies of suspension cells in transmission electron microscopy. J. Vis. Exp. 54874. https://doi.org/10.3791/54874.
97. Bochud-Allemann, N., and Schneider, A. (2002). Mitochondrial substrate level phosphorylation is essential for growth of procyclic Trypanosoma brucei. J. Biol. Chem. *277*, 32849–32854. https://doi.org/10.1074/jbc.M205776200.

Please cite this article in press as: Morel et al., A new member of the dynamin superfamily modulates mitochondrial membrane branching in *Trypanosoma brucei*, Current Biology (2025), https://doi.org/10.1016/j.cub.2025.02.033





## STAR★METHODS

### KEY RESOURCES TABLE

| REAGENT or RESOURCE | SOURCE | IDENTIFIER |
|---|---|---|
| **Antibodies** | | |
| Mouse anti-Ty1 | Gift of K. Gull; Bastin et al.[74] | N/A |
| Rabbit anti-Prohibitin | Gift of J. Lukeš; Tyc et al.[75] | N/A |
| Rabbit anti-Enolase | Gift of P. Michels; Hannaert et al.[37] | N/A |
| Rabbit anti-Atom40 | Gift of A. Schneider; Mani et al.[76] | N/A |
| Rabbit anti-Fumarate reductase glycosomal (Frdg) | Gift of F. Bringaud; Besteiro et al.[77] | N/A |
| Mouse anti-HSP60 clone H7 | Gift of F. Bringaud; Bringaud et al.[78] | N/A |
| Rabbit anti-Pyruvate Phosphate DiKinase (PPDK) | Gift of F. Bringaud; Bringaud et al.[79] | N/A |
| Rabbit anti-Threonine dehydrogenase (Tdh) | Gift of F. Bringaud; Millerioux et al.[35] | N/A |
| Rabbit anti-GFP | Abcam | Catalog #ab290 |
| Mouse anti-HA.11 | BioLegend | Catalog #901516 |
| Rat anti-HA High Affinity | Roche | Catalog #11867423001 |
| Goat anti-Mouse-HRP | Sigma-Aldrich | Catalog #A5278 |
| Goat anti-Rabbit-HRP | SeraCare | Catalog #074-15-061 |
| Donkey anti-Mouse Alexa fluor 594 | Thermofisher | Catalog #A-1105 |
| Donkey anti-Mouse Alexa fluor 488 | Thermofisher | Catalog #A-21202 |
| Donkey anti-Rabbit Alexa fluor 594 | Thermofisher | Catalog #A-11012 |
| Donkey anti-Rabbit Alexa fluor 488 | Thermofisher | Catalog #A-21206 |
| Donkey anti-Rat Alexa fluor 594 | Thermofisher | Catalog #A-21209 |
| Anti-Mousse IgG gold | British BioCell International | Catalog #EM.GAM10 |
| **Bacterial and virus strains** | | |
| XL1-blue | Avantor | Catalog #AGLS200249 |
| **Chemicals, peptides, and recombinant proteins** | | |
| Proteinase K | Sigma-Aldrich | Catalog #P6556-100MG |
| Digitonin | Sigma-Aldrich | Catalog #D141-500MG |
| Phenylmethanesulfonyl fluoride (PMSF) | Roche | Catalog #10837091001 |
| Triton X-100 solution | Sigma-Aldrich | Catalog #T8787-250ML |
| Rhodamine 123 | Sigma-Aldrich | Catalog #83702-10MG |
| Hoechst 33342 | Sigma-Aldrich | Catalog #B2261-25MG |
| DAPI | Sigma-Aldrich | Catalog #D9542-10MG |
| Paraformaldehyde 32% | Electron Microscopy Sciences | Catalog #15714 |
| **Critical commercial assays** | | |
| Clarity western enhanced-chemiluminescence | Bio-Rad | Catalog #1705060 |
| NucleoSpin Blood | Macherey-Nagel | Catalog #740951.250 |
| MitoTracker Green FM | Invitrogen | Catalog #M7514 |
| Cas9 enzyme | Integrated DNA Technologies | Catalog #1081059 |
| Basic Parasite Nucleofector Kit 2 | Lonza | Catalog #VMI-1021 |
| SlowFade Gold antifade reagent | Thermofisher | Catalog #S 36836 |
| **Deposited data** | | |
| Additional data have been deposited in an online data repository (Mendeley) | This paper | https://doi.org/10.17632/jr3jbf6fp8.1 |
| **Oligonucleotides** | | |
| For oligonucleotides used in this study: see Table S2 | Integrated DNA Technologies | N/A |

(*Continued on next page*)

Please cite this article in press as: Morel et al., A new member of the dynamin superfamily modulates mitochondrial membrane branching in *Trypanosoma brucei*, Current Biology (2025), https://doi.org/10.1016/j.cub.2025.02.033



*Continued*

| REAGENT or RESOURCE | SOURCE | IDENTIFIER |
|---|---|---|
| Recombinant DNA | | |
| pLew100 | Wirtz et al.[80] | N/A |
| pPOTv7 | Paterou et al.[81] | N/A |
| p2T7-177 | Wickstead et al.[82] | N/A |
| pHD1336 | Biebinger et al.[83] | N/A |
| Software and algorithms | | |
| GraphPad Prism 9 | GraphPad | https://www.graphpad.com/ |
| Image Lab V6.1 | Bio-Rad | https://www.bio-rad.com |
| Geneious R11 | Biomatters | https://www.geneious.com/ |
| Fiji | Schindelin et al.[84] | https://imagej.net/software/fiji/ |
| Metamorph V7 | Molecular Devices | https://www.moleculardevices.com/ |

## EXPERIMENTAL MODEL AND STUDY PARTICIPANT DETAILS

The procyclic form (PCF) of *T. brucei* EATRO1125.T7T (TetR-HYG-T7RNAPOL-NEO, where TetR stands for tetracycline resistance, HYG for hygromycin, T7RNAPOL for RNA polymerase T7, and NEO for neomycin) was cultured at 27°C with 5% $CO_2$ in SDM79 medium containing 10% (vol/vol) heat-inactivated fetal calf serum, 5 μg/ml hemin, 25 μg/ml hygromycin and 10 μg/mL neomycin. Procyclic form cells were also cultured in SDM80 medium containing either glucose (10 mM) as the sole carbon source or proline (5 mM) supplemented with N-acetyl-glucosamine (50 mM) to inhibit the glucose transporter. The bloodstream form (BSF) of *T. brucei* 427 90-13 (TetR-HYG-T7RNAPOLNEO) was cultured at 37°C with 5% $CO_2$ in Iscove's modified Dulbecco's medium (IMDM) supplemented with 10% (vol/vol) heat-inactivated fetal calf serum, 0.2 mM β-mercaptoethanol, 36 mM $NaHCO_3$, 1 mM hypoxanthine, 0.16 mM thymidine, 1 mM sodium pyruvate, 0.05 mM bathocuproine, 1.5 mM L-cysteine,[85] 5 μg/ml hygromycin and 2.5 μg/mL neomycin. Overexpression cell lines were induced with tetracycline (10 μg/mL for BSF and 1 μg/mL for PCF). Growth was monitored by daily cell counting with the cytometer Guava Muse and Guava easyCyte.

## METHOD DETAILS

### Sequence database searches and phylogenetic analysis

Two databases were used to identify sequences homologous to the *T. brucei Tb*MfnL sequence (VEuPathDB: Tb927.7.2410). The first search was conducted using Blastp[86] (protein-protein BLAST, https://blast.ncbi.nlm.nih.gov/Blast.cgi) on the NCBI non-redundant protein database, with *Tb*MfnL as the query and kinetoplastids excluded from the search. The parameters included a maximum of 5000 target sequences and the Blosum62 matrix. For the EuKProt v3 database[87] search (https://evocellbio.com/eukprot/), the BLASTp server was used with the entire database (993 species) and *Tb*MfnL as the query, without applying advanced parameters. The selection of sequences was then performed manually, retaining only those sequences that exhibited homology across the entire *Tb*MfnL protein. Sequences corresponding solely to the highly conserved GTPase domain were excluded. A total of 315 sequences were selected for phylogenetic analysis. An additional 23 sequences were included from well-characterized dynamins involved in fission (Dnm1), fusion (Opa1, Mfn1/2, Fzo1), BDLP (the cyanobacterial Mfn homolog), and dynamins associated with clathrin-mediated endocytosis (Dyn1/2) to be used as an outgroup.

The sequences were aligned with MAFFT L-INS-I v7.450[88] and trimmed with BMGE v1.12 (-m BLOSUM30 -b 3 -g 0.2 -h 0.5).[89] A maximum likelihood phylogenetic tree was then reconstructed with IQ-TREE v.2.0.3[90] using its model finder (-m TEST) option, including complex mixture models, to select the best fit substitution model, as well as 1000 ultrafast bootstrap replicates to estimate branch statistical support.

### Structural prediction software and sequence analysis

Structure predictions were performed using PSIPRED ("http://bioinf.cs.ucl.ac.uk/psipred/")[32] and prediction of mitochondrial targeting sequences by various algorithms (MitoFates, PSORT II and TargetP-2.0).[91]

### Endogenous tagging and inactivation of *Tb*MfnL by CRISPR-Cas9

Endogenous tagging and inactivation of *Tb*MfnL were achieved by CRISPR Cas9 technology.[39] Briefly, inactivation of the *Tb*MfnL was achieved by inserting the resistant marker puromycin (Pac) or a small sequence encoding for a *Bam*HI restriction site plus 6 successive stop codons, flanked by 50 bp homologous to the 5' and 3' *Tb*MfnL sequences from the Cas9 cutting site. Similar approaches have been performed for endogenous tagging with the insertion of a sequence encoding 3xTy1 or 3xHA. The EATRO1125.T7T procyclic form and the 427 90.13 bloodstream form ($1x10^6$ cells) were respectively transfected, using Amaxa

Please cite this article in press as: Morel et al., A new member of the dynamin superfamily modulates mitochondrial membrane branching in *Trypanosoma brucei*, Current Biology (2025), https://doi.org/10.1016/j.cub.2025.02.033



nucleofectorII, with 1 μg of purified cassette (puromycin resistance marker, Stop*Bam*H1Stop, 3xTy1 or 3xHA), 30 μg Cas9 protein from IDT and pre-annealing TracrRNA (0.4 μmol) and crRNA (0.4 μmol). Cells were transfected using program X-001 and selected or not with puromycin (SDM79, 1 μg/mL, or IMDM 0.1 μg)/mL). Cells were cloned by using a cell sorter (TBM Core facility), and selection of double inactivated *Tb*MfnL gene (*Tb*MfnL$^{-/-}$) or endogenously tagged clones was done by DNA extraction, with NucleoSpin Blood (Macherey-Nagel) and PCR amplification, see Table S2. Guide RNAs were designed using EuPaGDT, from http://tritrypdb.org. Primers and guide RNAs used were synthetized by Integrated DNA Technologies (IDT) and are listed in Table S2.

### Immunofluorescence

Cells were washed twice with PBS, then fixed with 2% paraformaldehyde (PFA) for 10 min at room temperature and 0.1mM glycine was added 10 min to stop the reaction. The cells were spread on slides and permeabilized with 0.05% triton X-100. After incubation in PBS containing 4% bovine serum albumin (BSA) 20 min, cells were incubated for 1 hour with primary antibodies diluted in PBS-BSA 4%, washed 4 times with PBS and incubated for 45 min with secondary antibodies diluted in PBS-BSA 4% followed by three washes. Then, kinetoplasts and nuclei were labelled with DAPI (10 μg/mL) for 5 min. Slides were washed 3 times with PBS and mounted with SlowFade Gold (Molecular probes). Images were acquired with MetaMorph software on Zeiss Imager Z1 or an Axioplan 2 microscope and processed with Fiji/ImageJ. Antibodies used in this study were: Anti-Ty1 (1:500), anti-HA (1:1000), anti-Tdh (1:200), anti-Hsp60 H7 (1:500), anti-Mouse Alexa fluor 594 (1:400), anti-Mouse Alexa fluor 488 (1:400), anti-Rabbit Alexa fluor 594 (1:400), anti-Rabbit Alexa fluor 488 (1:400) and anti-Rat Alexa fluor 594 (1:400).

### Mitochondria staining in live cells

Rhodamine-123 (30 μg/mL) was added on cell culture (5x10$^6$ - 1x10$^7$ cells per mL) for 15 min at room temperature, then cells were washed twice with PBS and spread on slides. As an alternative to labeling mitochondria in living cells with Rhodamine-123, Mitotracker (MitoTracker Green FM) was used. Cells were washed once with PBS, incubated for 10 minutes with 10 μM MitoTracker Green FM, washed again with PBS, and then spread onto slides. Images were acquired with MetaMorph software on an Axioplan 2 microscope and processed with Fiji/ImageJ.

### Ultrastructure Expansion Microscopy (UExM)

The protocol of UExM was realized exactly as described by Casas et al.[92] An expansion factor was determined using the ratio between the size of the coverslip (12 mm) and the size of the gels after the first expansion. Images were acquired on a confocal Leica SP5-MP (Bordeaux Imaging Center) using a 63X oil objective and processed with Fiji/ImageJ. Antibodies used in this study were: Anti-Ty1 (1:250), anti-HA (1:500), anti-Tdh (1:100), anti-Mouse Alexa fluor 594 (1:250), anti-Mouse Alexa fluor 488 (1:250), anti-Rabbit Alexa fluor 594 (1:250) and anti-Rabbit Alexa fluor 488 (1:250).

### Quantification of Mitochondrial junctions - ImageJ macro

To quantify the number of mitochondrial junctions, an ImageJ macro was developed with the help of the Bordeaux Imaging Center (BIC). The script is presented in supplemental (Methods S1).

### Endogenous tagging and overexpression of *Tb*MfnL

For endogenous gene tagging, primers were designed as described in Dean et al.[93] and PCR was performed using pPOTv7 vector as template. The pPOT used here was pPOTv7 for C-terminus 10xHA tagging (blasticidin resistance). For overexpression, *MfnL* gene (VEuPathDB: Tb427.7.2410) was inserted in both pLew100 (phleomycine resistance)[80] and pHD1336 (blasticidin resistance)[83] expression vectors. Fragments were amplified and cloned into *Hin*dIII and *Xba*I restrictions sites of the pLew100 and into *Hin*dIII and *Bam*HI restrictions sites of the pHD1336 expression vectors. In addition, a 3xTy1 tag was added at the C-terminus of the protein in the pLew100-*Tb*MfnL, using the *Xba*I and *Bam*HI restrictions sites. The truncated version of *Tb*MfnL without the first 41 amino acids (*Tb*MfnL-ΔMTS) and without the two trans-membranes domain (*Tb*MfnL-ΔTM) were amplified and cloned in the pLew100 with a 3xTy1 tag as previously described. Catalytic lysine (K141) was replaced by an alanine, using PCR approach[94] and PCR product cloned in the pLew100 with a 3xTy1 tag (*Tb*MfnL-K141A). EATRO1125.T7T procyclic form was transfected using Amaxa Nucleofector II, program X-001 and selected in SDM79 containing 25 μg/ml hygromycin 10 μg/mL neomycin and 5 μg/mL phleomycin. 427 90-13 bloodstream form was transfected using the same conditions and selected in IMDM containing 5 μg/ml hygromycin, 2.5 μg/mL neomycin and 5 μg/mL blasticidin. Primers used for the constructions are presented in the Table S2.

### Down-regulation of *Tb*MfnL gene expression

Down-regulation of *Tb*MfnL expression by RNAi in procyclic form was achieved by expression of stemloop "sense/antisense" RNA molecules targeting a 400-bp fragment of the *Tb*MfnL gene introduced into the pLew100 tetracycline-inducible expression vector. A PCR-amplified 450-bp fragment, containing the antisense *Tb*MfnL sequence was inserted between *Xho*I and *Bam*HI restriction sites of the pLew100 plasmid. Then, the separate 400-bp PCR-amplified fragment containing the sense *Tb*MfnL sequence was inserted upstream of the antisense sequence, using *Hin*dIII and *Xho*I restriction sites. The resulting plasmid, pLew100-*Tb*MfnL-SAS, contains a sense and antisense version of the *Tb*MfnL fragment separated by a 50-bp fragment. The EATRO1125 procyclic form was transfected with the pLew100-*Tb*MfnL-SAS and cells were selected in SDM79 medium containing 25 μg/ml hygromycin, 10 μg/mL neomycin and 5 μg/mL phleomycin. Expression of the RNAi was induced by tetracycline (1 μg/mL). Down-regulation of *Tb*MfnL

Please cite this article in press as: Morel et al., A new member of the dynamin superfamily modulates mitochondrial membrane branching in *Trypanosoma brucei*, Current Biology (2025), https://doi.org/10.1016/j.cub.2025.02.033



expression by RNAi in bloodstream form was achieved exactly as described[30] with a 280-bp fragment derived from the *Tb*MfnL open reading frame inserted into the p2T7-177 plasmid.[82] Linearized plasmid was transfected in *T. brucei* 427 90-13 (TetR-HYG-T7RNAPOL-NEO) bloodstream form cells. Expression of the RNAi was induced by tetracycline (10 μg/mL). Primers used for the constructions are presented in Table S2.

### Serial Block-Face Scanning Electron Microscopy (SBF-SEM)

The entire procedure is detailed and has been carried out as described in the article: Advancing yeast cell analysis: A cryomethod for serial block-face scanning electron microscopy imaging in mitochondrial morphology studies.[95]

### Immunoelectron microscopy

Harvested cells were placed on the surface of formvar-coated copper grids (400 mesh). Each loop was quickly submersed in liquid propane (−180°C) and transferred into a precooled solution of 0.1% uranyl acetate in dry acetone for 3 days at -82°C. Samples were rinsed with acetone at -20°C and embedded progressively at -20°C in LR Gold resin (EMS, USA). Resin polymerization was carried out at -20°C for 7 days under UV illumination. Ultrathin LR Gold sections were collected on nickel grids coated with formvar. Sections were first incubated for 15 min with 500mM $NH_4Cl$ in Tris-buffered saline (TBS) pH7.8, blocked 2x10 min with 2% BSA in TBS pH 7.8. The grids were incubated 1 hour at room temperature with anti Ty1 antibody diluted to 1:200 in TBS containing 2% BSA rinsed with TBS containing 2% BSA and with TBS containing 1% BSA. The samples were then incubated for 1 hour at room temperature with anti-mouse IgG diluted to 1:20 conjugated to 10 nm gold particles (British BioCell International). The sections were rinsed with TBS containing 1% BSA, and fix with 1% glutaraldehyde in TBS. After rinsing with TBS, grids were contrasted through a 5 min incubation with 2% uranyl acetate in water, followed by 1 min incubation with 1% lead citrate. Observations were performed on a HITACHI H7650 transmission electron microscope operated at 80 KV with an Orius 1000-11 MPx camera (Gatan, Abingdon, UK).

### Transmission electron microscopy (TEM)

The entire procedure is thoroughly detailed and has been carried out precisely as described in the article: Plunge Freezing: A Tool for the Ultrastructural and Immunolocalization Studies of Suspension Cells in Transmission Electron Microscopy.[96]

### Western blot analyses and quantification

Total protein extracts ($5x10^6$ cells) were separated by SDS-PAGE (10%) and immunoblotted on TransBlot Turbo Midi-size PVDF Membranes (Bio-Rad). Immunodetection was performed using the primary antibodies, diluted in PBS-Tween Milk (0.05% Tween20, 5% skimmed milk powder), summarized in the key resources table. Revelation was performed using a second antibody coupled to the horseradish peroxidase and the Clarity western enhanced-chemiluminescence (ECL) substrate as describes by the manufacturer (Bio-Rad). Images were acquired and analyzed with the ImageQuant Las 4000 luminescent image analyzer. Band intensities were quantified by measuring the band areas with ImageJ software and were normalized to the loading control. Antibodies used in this study were: Anti-Ty1 (1:1000), anti-HA (1:1000), anti-Tdh (1:500), anti-Enolase (1:100000), anti-Atom40 (1:1000), anti-Frdg (1:50), anti-PPDK (1:1000), anti-GFP (1:1000), anti-Prohibitin (1:1000), anti-mouse HRP (1:5000) and anti-Rabbit HRP (1:10000).

### Mitochondria-enriched preparation, proteinase K protection assays and carbonate extraction

This procedure has been well established and allows the determination of the submitochondrial localization of trypanosome proteins.[47,48,97] $10^8$ cells were lysed in SoTE buffer (20 mM Tris-HCl, pH 7.5, 0.6 mL sorbitol, and 2 mM ethylenediaminetetraacetic acid), supplemented with 0.02% (w/v) digitonin for 5 min at 4°C. A portion of the resulting suspension was collected as the total fraction (TF), while the remaining suspension underwent centrifugation at 6,000 x g for 3 minutes at 4°C to isolate a mitochondria-enriched pellet. This pellet was then resuspended in SoTE supplemented with 0.2% (w/v) digitonin and incubated on ice for 15 minutes. The resuspended mixture was divided into three tubes and subjected to centrifugation at 6,000 × g for 3 minutes at 4°C, resulting in the separation of mitoplasts and soluble protein in the supernatant (S). Each mitoplast pellet was resuspended in SoTE and subjected to the proteinase K protection assay. Proteinase K (50 μg) was added to two tubes, one supplemented with 1% Triton-X100 (v/v), while the third tube remained untreated as a control. All tubes were then incubated on ice for 30 minutes, followed by addition of 5 mM phenylmethanesulfonyl fluoride to stop the reaction. Proteins from all fractions were precipitated with trichloroacetic acid before undergoing resolution by SDS-PAGE.

For the extraction of integral membrane proteins using the carbonate method, the procedure begins with a mitochondria-enriched pellet. The pellet is resuspended in 500 μL of 10 mM $MgCl_2$ and subjected to a freeze-thaw cycle repeated ten times, involving freezing in liquid nitrogen and thawing at room temperature. Subsequently, the suspension is divided into two fractions: 50 μL and 450 μL. The 450 μL fraction is centrifuged at 10,000 × g for 5 minutes at 4 °C, with the supernatant designated as the matrix fraction. The 50 μL fraction is centrifuged under the same conditions, and the resulting pellet is resuspended in 50 μL of 10 mM $MgCl_2$, representing the membrane fraction. The remaining pellet from the 450 μL sample is further processed by resuspending it in 400 μL of 0.1 M $Na_2CO_3$ (pH 11). This mixture is incubated on ice for 30 minutes, sonicated four times, and centrifuged at 20,000 × g for 20 minutes at 4 °C. The supernatant is collected as the peripheral membrane protein fraction. The pellet is washed by resuspension in 400 μL of 0.1 M $Na_2CO_3$ and subjected to another centrifugation under the same conditions. This final pellet constitutes the integral membrane protein fraction. All protein fractions are precipitated using trichloroacetic acid, resuspended in 50 to 100 μL of 2% SDS, and analyzed by SDS–PAGE.

Please cite this article in press as: Morel et al., A new member of the dynamin superfamily modulates mitochondrial membrane branching in *Trypanosoma brucei*, Current Biology (2025), https://doi.org/10.1016/j.cub.2025.02.033





## QUANTIFICATION AND STATISTICAL ANALYSIS

### Statistical analysis

Experiments were performed at least in triplicates. Statistical analyses were performed using Prism (GraphPad) software. The results are presented as mean ± S.D. Where indicated the results were subjected to two-sided Student's t-test to determine statistical differences against the indicated group (ns: $p \geq 0.05$; *: $p<0.05$; **: $p<0.01$; ***: $p<0.001$).